Available online at www.sciencedirect.com
SCIENCE DIRECT®
ELSEVIER
Earth and Planetary Science Letters 240 (2005) 95–121
EPSL
www.elsevier.com/locate/epsl

Provenance and diagenesis of the evaporite-bearing Burns formation, Meridiani Planum, Mars

S.M. McLennan [a,*], J.F. Bell III [b], W.M. Calvin [c], P.R. Christensen [d], B.C. Clark [e], P.A. de Souza [f,g], J. Farmer [d], W.H. Farrand [h], D.A. Fike [i], R. Gellert [f,j], A. Ghosh [k], T.D. Glotch [d], J.P. Grotzinger [i], B. Hahn [a], K.E. Herkenhoff [l], J.A. Hurowitz [a], J.R. Johnson [l], S.S. Johnson [i], B. Jolliff [m], G. Klingelhöfer [f], A.H. Knoll [n], Z. Learner [b], M.C. Malin [o], H.Y. McSween Jr. [k], J. Pocock [c], S.W. Ruff [d], L.A. Soderblom [l], S.W. Squyres [b], N.J. Tosca [a], W.A. Watters [i], M.B. Wyatt [d], A. Yen [p]

[a] *Department of Geosciences, State University of New York at Stony Brook, Stony Brook, NY 11794-2100, USA*
[b] *Department of Astronomy, Space Sciences Bldg. Cornell University, Ithaca, NY 14853, USA*
[c] *University of Nevada, Reno, Geol. Sci., Reno, NV 89557, USA*
[d] *Department of Geological Sciences, Arizona State University, Tempe, AZ 85287, USA*
[e] *Lockheed Martin Corporation, Littleton, CO 80127, USA*
[f] *Institut für Anorganische und Analytische Chemie, Johannes Gutenberg-Universität, Staudinger Weg 9, D-55128 Mainz, Germany*
[g] *CVRD Group, Vitoria, Brazil*
[h] *Space Science Institute, Boulder, CO 80301, USA*
[i] *Massachusetts Inst. of Technology, Earth, Atmos. and Planetary Sci., Cambridge, MA 02139, USA*
[j] *Max-Planck-Institut für Chemie, J. J. Becher-Weg 27, D-55128 Mainz, Germany*
[k] *Department of Earth and Planetary Sciences, Univ. of Tennessee, Knoxville Tennessee 37996, USA*
[l] *U.S. Geological Survey, Flagstaff, AZ 86001, USA*
[m] *Department Earth and Planetary Sciences, Washington University, St. Louis, MO 63130, USA*
[n] *Botanical Museum, Harvard University, Cambridge MA 02138, USA*
[o] *Malin Space Science Systems, San Diego, CA 92191, USA*
[p] *Jet Propulsion Laboratory, California Institute of Technology, Pasadena, CA 91109, USA*

Accepted 22 September 2005
Available online 25 October 2005
Editor: A.N. Halliday

Abstract

Impure reworked evaporitic sandstones, preserved on Meridiani Planum, Mars, are mixtures of roughly equal amounts of altered siliciclastic debris, of basaltic provenance (40 ± 10% by mass), and chemical constituents, dominated by evaporitic minerals (jarosite, Mg-, Ca-sulfates ± chlorides ± Fe-, Na-sulfates), hematite and possibly secondary silica (60 ± 10%). These chemical constituents and their relative abundances are not an equilibrium evaporite assemblage and to a substantial degree have been reworked by aeolian and subaqueous transport. Ultimately they formed by evaporation of acidic waters derived from interaction with olivine-bearing basalts and subsequent diagenetic alteration. The rocks experienced an extended diagenetic history, with at least two and up to four distinct episodes of cementation, including stratigraphically restricted zones of recrystallization and

* Corresponding author. Tel.: +1 631 632 8194; fax: +1 631 632 8240.
E-mail address: scott.mclennan@sunysb.edu (S.M. McLennan).

0012-821X/$ - see front matter
doi:10.1016/j.epsl.2005.09.041

secondary porosity, non-randomly distributed, highly spherical millimeter-scale hematitic concretions, millimeter-scale crystal molds, interpreted to have resulted from dissolution of a highly soluble evaporite mineral, elongate to sheet-like vugs and evidence for minor synsedimentary deformation (convolute and contorted bedding, possible teepee structures or salt ridge features). Other features that may be diagenetic, but more likely are associated with relatively recent meteorite impact, are meter-scale fracture patterns, veins and polygonal fractures on rock surfaces that cut across bedding. Crystallization of minerals that originally filled the molds, early cement and sediment deformation occurred syndepositionally or during early diagenesis. All other diagenetic features are consistent with formation during later diagenesis in the phreatic (fluid saturated) zone or capillary fringe of a groundwater table under near isotropic hydrological conditions such as those expected during periodic groundwater recharge. Textural evidence suggests that rapidly formed hematitic concretions post-date the primary mineral now represented by crystal molds and early pore-filling cements but pre-date secondary moldic and vug porosity. The second generation of cements followed formation of secondary porosity. This paragenetic sequence is consistent with an extended history of syndepositional through post-depositional diagenesis in the presence of a slowly fluctuating, chemically evolving, but persistently high ionic strength groundwater system.

Keywords: Mars; Meridiani Planum; diagenesis; geochemistry; sedimentology; provenance

1. Introduction

Preserved on the plains of Meridiani Planum, in the vicinity of the *Opportunity* Rover landing site, are sedimentary rocks, at least 7 m thick, interpreted to represent a succession of reworked impure evaporitic sandstones [1,2]. *Opportunity* has traced these rocks over more than 2 km laterally and orbital data suggest that the sequence and its direct correlatives may extend over several hundred thousand square kilometers [3–5]. Stratigraphic relationships and sedimentary structures indicate that depositional environments include a combination of aeolian and shallow water conditions, such as those commonly found in aeolian dune—sand sheet—interdune environments [1,2].

Only limited insight into the origin of evaporitic rocks on Mars can be obtained from the study of terrestrial analogs. The martian upper crust is dominated by basalt (e.g., [6–8]) and thus siliciclastic material admixed with chemical components can be expected to be of basaltic provenance. Few terrestrial studies exist to guide the evaluation of such source rocks [9–13]. Similarly, any water from which evaporitic minerals precipitate is likely to have interacted almost exclusively with basaltic rocks, rather than more petrologically evolved (e.g., granitic) igneous rocks and their sedimentary/metamorphic derivatives typical of the terrestrial upper continental crust. Thus, Meridiani water chemistry and its expected evaporitic sequences are likely to differ fundamentally from most evaporites encountered on Earth [14–17].

A variety of remarkably well-preserved textures indicate that these sedimentary rocks have undergone an extended diagenetic history [1,2,18,19]. Included are multiple phases of cementation, stratigraphic zones of recrystallization, formation of spherules, crystal molds and other secondary porosity, small-scale deformation features, and, less clearly diagenetic, fractures, veins and polygonal structures. Understanding the origin of these features and their relative timing are central to a full evaluation of the geological history of these sedimentary rocks and a satisfactory understanding of the history of aqueous activity in this region. No evidence of biological activity has been found at Meridiani Planum but on Earth such sedimentary environments support life and preserve physical and/or chemical biosignatures in accumulating sediments [20]. Sedimentary reworking and mixing may well obscure any such evidence, whereas certain diagenetic processes can either disrupt (e.g., recrystallization) or enhance (e.g., concretion formation) fossil preservation potential. Accordingly, the purpose of this paper is to evaluate the provenance and diagenesis of sedimentary rocks encountered in the vicinity of the *Opportunity* landing site on Meridiani Planum.

2. Geological and sedimentological setting

A summary of the geological setting of Meridiani Planum is provided by Grotzinger et al. [2; also see 3]. Hematite-bearing deposits of Meridiani Planum, which include the sedimentary rocks examined by *Opportunity*, appear to be part of the uppermost unit of a layered complex that extends over an area of at least 200,000 km^2. Although its geological age is not well established, it is likely of late Noachian or early Hesperian age and thus in excess of about 3.5 Ga [21].

Approximately 7 m of stratigraphic section have been studied in some detail at four locations [22,23] including, from west to east, Eagle crater (upper < 1 m of preserved stratigraphy), Anatolia depression (upper < 1 m), Fram crater (upper < 1 m) and Endurance crater

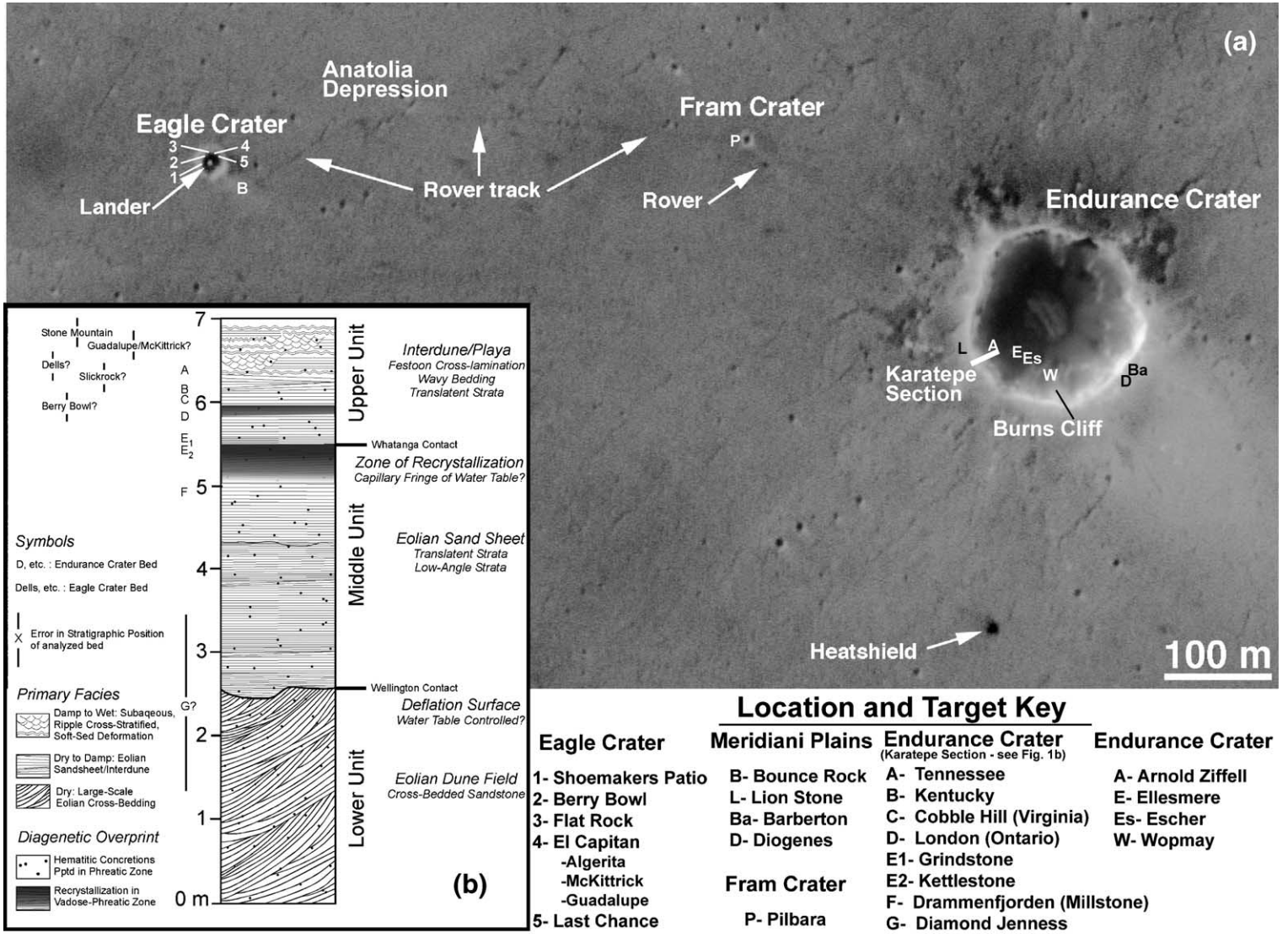

Fig. 1. Location and stratigraphic relationships of the Burns formation on Meridiani Planum Mars. (a) Mars Orbital Camera (MOC) image of the Opportunity landing area showing the location of major craters and features discussed in the text. Image was taken on 26 April, 2004 (*Opportunity* Sol 91) and is a subframe of MOC image R16-02188 with a resolution of 0.5m/pixel). (b) Stratigraphic relationships of the Burns formation (see [2] for full description) showing the stratigraphic position of many of the targets and analyses discussed in the text. Figure adapted from Grotzinger et al. [2].

(~7 m). At the time of writing, *Opportunity* is carrying out a long traverse to the south of Endurance crater in an attempt to extend the lateral and stratigraphic extent of these sedimentary rocks.

Squyres et al. [1] and Grotzinger et al. [2] have discussed the stratigraphic and sedimentological settings of these rocks. Grotzinger et al. [2] *informally* named this sequence the "Burns formation" and divided it into lower, middle and upper units. The unit is named after the Burns Cliff within Endurance crater, which in turn is named in honor of the late Roger Burns, a renowned planetary scientist [24]. The lower unit, characterized by high angle planar cross beds, is interpreted to represent an aeolian dune facies. The sharp contact (Wellington contact) that separates lower and middle units appears to be a deflation surface controlled by the position of a paleo-water table. Low angle strata of the middle unit are thought to represent an aeolian sand sheet facies. The contact between the middle and upper units is not a facies boundary but rather a zone of recrystallization within the sand sheet facies (Whatanga contact) interpreted to represent the capillary fringe of a stagnant paleo-water table and thus a diagenetic boundary. The upper unit grades upward from the sand sheet facies into sedimentary rocks characterized by more complex bedforms including small-scale festoon cross-lamination and wavy bedding, the former being diagnostic of deposition by water currents. This unit, accordingly, is interpreted to represent an intermittently damp to wet interdune facies. No textural evidence has been found for crystallization of evaporite minerals within or at the bottom of a free-standing water column and all of these rocks appear to have been reworked by aeolian or subaqueous currents.

The locations of major features, rocks and other targets that are discussed in this paper are shown in Fig. 1. Fig. 1a is a Mars Orbital Camera image of the *Opportunity* landing site and vicinity showing craters and the major features and rocks encountered on the Meridiani Plains and discussed in this paper. Fig. 1b is a composite stratigraphic section of the Burns formation from Grotzinger et al. [2] showing the stratigraphic position of many of the analyzed targets.

3. Constraints on bulk mineralogy

No petrographic or textural evidence has been found that unambiguously identifies any mineral. In places, near-euhedral pores exist that appear to have monoclinic crystal forms (see below). The best constraints on mineralogy of pristine Meridiani outcrops come from a combination of chemical composition and Mössbauer spectroscopy of abraded rock surfaces (using the RAT, rock abrasion tool), thermal emission infrared spectroscopy (Mini-TES) of rock surfaces and visible through near infrared panoramic camera (Pancam) images. Clark et al. [25; also see 26–28] summarized the geochemistry and mineralogy of these sedimentary

Table 1
Constraints on mineralogy of the Burns formation

Mineral[+]	Weight %	Comment
Chemical Constituents	60 ± 10	From S and Cl mass balance.
Hematite	6	35-40% of iron as hematite from Mössbauer. At least one-half of hematite is in spherules.
Jarosite*	10	20-35% of iron as jarosite from Mössbauer.
Mg-Sulfate*	18 ± 5	From variation associated with Mg and S correlation; Mini-TES spectrum best fit with Mg-and Ca-sulfates.
Other Sulfates*	10 ± 5	From S mass balance; likely to include Ca-and possibly other Fe-sulfates; Mini-TES spectrum best fit with Mg-and Ca-sulfates.
Chlorides	≤2	Possible presence based on Cl abundance; Cl may not be separate mineral but solid solution with sulfate or mixed anion salt.
Secondary Silica	15 ± 10	Presence is inferred from geochemical mass balance (e.g., Si/Al ratios) which indicates as much as 25%; Mini-TES should detect if abundance >5-10%.
Siliciclastic Constituents	40 ± 10	Consistent with S, Cl mass balance and Al abundance.
Olivine	trace	From Mössbauer; may not be intrinsic to outcrop.
"Pyroxene"	5-10	From Mössbauer; assumes Fe contents typical of pyroxenes in SNC meteorites. The mineral assignment of pyroxene is not a unique interpretation for octahedrally coordinated Fe(II) and likely to be other phase(s).
Other	35 ± 5	Includes other igneous and altered igneous components and possibly sheet silicates; Fe-bearing components dominated by Fe(III) and so likely altered.

[+]-All mineralogical constraints are on a volatile-free basis. Chemical constituents likely are hydrated and so their proportions would accordingly be greater than indicated above.

*-Total sulfate mineralogy is constrained to be about 35–40% on an anhydrous basis based on SO_3 content, with exact amount depending on the mineralogy.

rocks. Both mineralogy and chemistry are remarkably uniform in the outcrop rocks and can be subdivided into roughly subequal amounts of chemical components ($60 \pm 10\%$ by mass), including: (1) sulfates, hematite, possibly chlorides and possibly secondary silica, and (2) siliciclastic components ($40 \pm 10\%$), likely dominated by basaltic debris, and its weathering products. The best quantitative constraints on mineralogy are provided in Table 1. Stratigraphic variations exist in the proportions of various minerals and in chemical composition; these are described in detail by Clark et al. [25]. The difficulty in relating mineralogy to textures imposes a

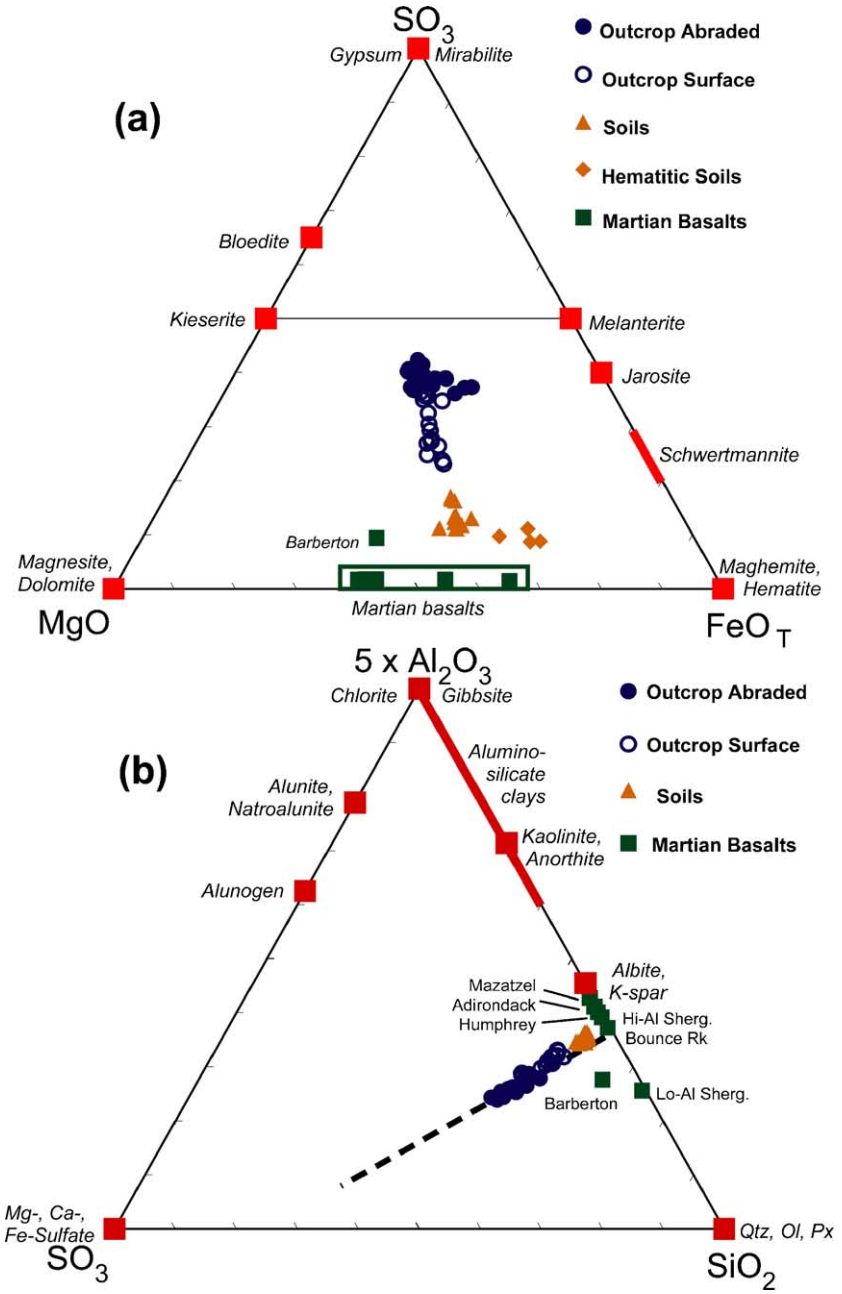

Fig. 2. (a) Plot of mole proportions SO_3 – MgO – FeO_T for abraded and unabraded outcrop and soils. Shown for reference are compositions of various end-member mineral compositions and various martian basaltic rocks (SNC meteorites, Gusev and Meridiani basalts; note that the basaltic cobble Barberton was not RATed and thus has significant amounts of sulfur due to dust and soil contamination). (b) Plot of mole proportions $Al_2O_3(\times 5)$ – SO_3 – SiO_2. Outcrop material forms a linear trend consistent with mixing between a siliciclastic basaltic provenance and a sulfate rich chemical component. Note that the trend intersects the SO_3 – SiO_2 join, consistent with a component of secondary silica.

first order source of uncertainty in interpreting these sedimentary rocks. Apart from field experiments carried out by *Opportunity*, which clearly indicate that spherules are composed of hematite ± basaltic debris ± minor sulfates (see below), no mineralogical identification or inference can be related unambiguously to any textural feature.

Chemical components are dominated by some combination of Mg-, Fe- and Ca-sulfates. The only sulfate mineral unambiguously identified by Mössbauer spectroscopy is jarosite (either mixed Na- and K-jarosite and/or hydronium jarosite), and makes up about 10% of the rocks. Occurrence of jarosite is particularly important because it is stable only under low pH conditions of about five or less [17,25]. On Earth, jarosite typically forms during acid–sulfate alteration of volcanic rocks or during pyrite alteration in acid mine drainage settings (e.g., [29,30]). However, on Mars where near surface water chemistry is likely to be dominated by basalt alteration, jarosite is also a plausible evaporite mineral under low pH conditions [15,17]. Mini-TES spectra of outcrops identified an absorption edge at 1250 cm^{-1}, consistent with the presence of sulfates. Spectral deconvolution, using a library consisting of various Ca-, Mg-, Na- and Fe-sulfates, indicates a best fit for a mixture of Ca- and Mg-sulfates [28].

Chlorine is not so high (0.3–1.3%) as to demand separate chloride phases and may simply substitute in dominantly sulfate or mixed sulfate-chloride minerals. On the other hand, Br/Cl ratios are highly variable [25,26] suggesting that late-forming evaporitic minerals, such as chlorides or bromides, may have formed in this geochemical system. Clark et al. [25] carefully evaluated the chemical mass balance and suggested that Mg- and Ca-chlorides are likely candidates.

Hematite constitutes about 6% of these rocks on average. Much of it is contained in spherules, but as much as one-half of the hematite may be dispersed throughout the outcrop (the exact amount depending on how much hematite is contained in spherules, a value that is not well constrained; see Section 5.2 below). The chemical composition remaining after removal of plausible chemical components suggests a basaltic composition, likely one that has been significantly altered. The various components that are identified or inferred can be illustrated on two ternary diagrams plotting mole fraction SO_3–MgO–FeO_T (Fig. 2a) and Al_2O_3(×5)–SO_3–SiO_2 (Fig. 2b). In Fig. 2a, the abraded outcrop analyses cluster near the center of the diagram, consistent with a mixture of both basaltic debris and a variety of chemical constituents. In Fig. 2b, outcrop rocks form a clear linear trend that intersects the Al_2O_3–SiO_2 join in the vicinity of typical martian basalts with relatively high SiO_2/Al_2O_3 ratios. The trend extrapolates to about 0.20–0.30 on the SO_3–SiO_2 join, consistent with about 5–8% secondary silica. On abraded outcrop surfaces, the amount of SiO_2 does not drop off with increasing SO_3 content at the same rate as other elements that are likely concentrated in the siliciclastic component (e.g., Al, Ti, K) also suggesting excess silica. Model-dependent geochemical mass balance calculations result in as much as 25% secondary silica [25].

Although these rocks have a fairly complex diagenetic history (see below) it is likely that most of the detrital sand grains are evaporite-cemented basaltic mud (see below) derived from penecontemporaneous playa lakes [2; also see below], suggesting that transported intrabasinal chemical (i.e., allochemical) components make up a significant fraction of the rocks (~25 ± 10%). Accordingly, these rocks are best described as impure allochemical sandstones [31].

4. Constraints on provenance

Provenance of these sedimentary rocks can be considered on three levels: origin of detrital grains, origin of the siliciclastic components, and source of chemical constituents.

4.1. Provenance of grains

Detailed examination of sedimentary textures indicates that these rocks are fine to medium-grained sandstones. Where well defined, the grains are mostly moderately well rounded fine to coarse sand sized, typically in the range of 0.1–1 mm. Grains smaller than about 0.08–0.10 mm cannot be resolved with the MI and so any mode of very fine sand or silt cannot be discerned. In any case, relatively uniform grain size distributions in individual MI images, and especially within individual laminae, suggest that these are well-sorted sandstones with individual laminae being very well sorted. Abraded outcrop surfaces reveal no textural evidence suggesting that grains are simply volcanic rock or relatively unaltered siliciclastic mineral fragments. For example, there are no systematic variations in albedo from grain to grain or from grain surfaces to grain interiors. Mössbauer results indicate that Fe^{3+}/Fe_T ratios are in the range of 0.85–0.90 for abraded outcrop surfaces suggesting that the bulk of Fe-bearing siliciclastic components making up grains is composed largely of altered material. Evidence for any primary igneous minerals in Mössbauer spectra of

abraded outcrop surfaces is not especially compelling [27]. In abraded spherules, interpreted to be concretions (see below), no relict grain textures are preserved at MI resolution, so that any siliciclastic material remaining within the spherules must be very fine.

Accordingly, we interpret these grains to be derived from reworking of evaporite-cemented basaltic mud (grain sizes < 100 μm, the effective limit of resolution). The production of aeolian evaporitic sands, notably gypsum sands, is well documented in terrestrial playa lake environments (e.g., [32–36]). Evaporitic detritus can be derived from aeolian reworking of evaporite-cemented mud flats or efflorescent crusts that incorporate fine-grained siliciclastic debris. In the case of the Burns formation, the evaporitic sand grains probably are dominated by basaltic mud rather than evaporitic minerals themselves. An important implication of this model is that playa conditions must have been present at about the time of Burns formation deposition in order to provide the source of sand-sized particles.

Chemical constraints suggest that the siliciclastic component of these sedimentary rocks is between approximately 30–50% on an anhydrous basis and is likely concentrated within the grains, although some component of aeolian dust deposited during deposition of the Burns formation itself could also be present [37]. Thus, given that on the order of 35–45% of the sediment mass is composed of various sulfate ± chloride cements [25], a significant fraction of each of the grains is likely to be composed of evaporitic cements.

4.2. Provenance of siliciclastic component

Geochemical and mineralogical constraints clearly indicate that the siliciclastic provenance is composed predominantly of basaltic sources (Fig. 2). Although Mössbauer spectra on abraded surfaces indicate about 5–10% pyroxene and, at most, trace levels of olivine, the identification of pyroxene by Mössbauer is not definitive. This spectral feature could represent another octahedrally coordinated Fe(II) phase [27]. Mini-TES "footprints" are much larger than the area exposed by the RAT and so mineralogical determinations by this instrument are difficult to relate unambiguously to abraded outcrop. Nevertheless, dust-corrected mineralogical determinations on outcrop surfaces made by Mini-TES suggest the following non-chemical constituents (in approximate decreasing order): intermediate to high-silica components (modeled as high-Si glass, feldspar and minor sheet silicates), olivine and pyroxene [28]. However, correlating Mini-TES with Pancam images suggests that olivine and pyroxene abundances are strongly controlled by the presence of wind-blown sand on the outcrop surfaces and thus are likely not intrinsic to the Burns formation. In any case, no mineral has been identified or inferred from spectral data (e.g., quartz, K-feldspar, biotite, amphibole) that is inconsistent with a purely basaltic provenance or its altered derivative.

Characterizing the nature of the basaltic component is not straightforward. Because the mineralogy of chemical constituents is only partially constrained, it is not possible to evaluate the bulk chemistry of siliciclastic components quantitatively. Similarly, evaluating the degree to which siliciclastic material has been altered is difficult because variations in chemical composition that are characteristic of chemical weathering and low temperature alteration (e.g., [12]) cannot be disentangled from possible variations in evaporitic mineralogy. For example, partitioning of Ca, Mg, Fe, Na and K between chemical and non-chemical components is not known with certainty and so it is not possible to "remove" the chemical components through mass balance mixing calculation with any certainty. Even silicon, commonly released as amorphous silica in basalt alteration processes [38], does not necessarily reflect igneous abundances and indeed there is evidence that secondary silica is present (Fig. 2b; also see [25]). Accordingly, we are left with elements Al, Ti, Cr and Ni as most likely to reflect primary provenance relationships. However, it is worth noting that in low pH environments even Al is relatively mobile and that aluminum sulfates can be a common chemical constituent in acid lake and acid alteration environments (e.g., [30]).

Assuming that Al, Ti, Cr and Ni are reflective of the average provenance composition, no known martian basalt is a good match for the siliciclastic component of the Meridiani outcrop. The outcrop is characterized by modest Cr/Ni ratios of about 2 (Fig. 3) and high Ni abundances (730 ppm average); SNC meteorites and basalts from the other MER site at Gusev crater all have an order of magnitude higher Cr/Ni ratios. Of the two Meridiani igneous rocks analyzed (Bounce Rock and Barberton), only Barberton comes close to the Meridiani outcrops with comparable Cr/Ni ratios and only slightly higher Cr abundances (normalized to Al). However, Meridiani outcrop rocks have TiO_2/Al_2O_3 ratios that are more than 50% higher than Barberton and so the match is not exact. Chromium and nickel are highly susceptible to compositional variations associated with igneous fractionation of olivine and spinel and it is notable that many basaltic shergottites are cumulates. Accordingly, the basaltic provenance of the Meridiani

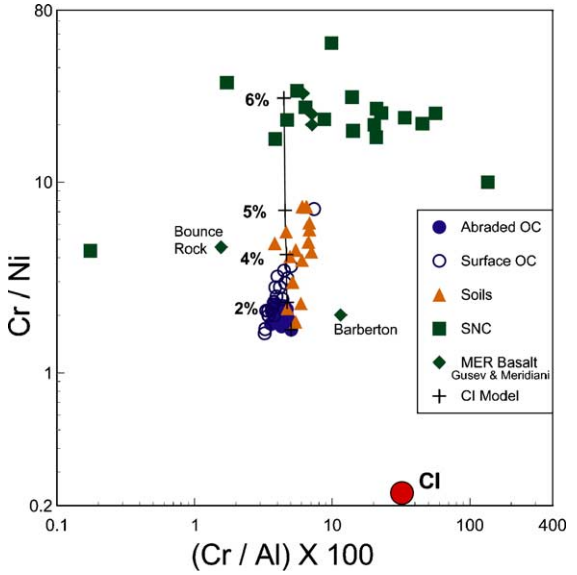

Fig. 3. Plot of Cr/Ni vs. Cr/Al(X100) for abraded outcrop rocks. Also shown are unabraded outcrop surfaces, Meridiani soils and basalt-ultramafic compositions from SNC meteorites, Gusev basalts and Meridiani basalts (Barberton and Bounce Rock). Note that only Barberton (which was too small to be abraded by the RAT) has Cr/Ni ratios and Cr/Al ratios that are within a factor of two of the Meridiani outcrop. Also shown is the effect of removing a composition equivalent to CI meteorites from outcrop compositions. Removal of about 6% of a meteoritic component moves the data into the field of typical SNC meteorites. However, the Cr-Ni-Al relationships of the outcrop are not so distinctive in comparison to known Mars basaltic compositions or basalts in general [42] as to demand a meteoritic component in the provenance.

outcrop could be related to one of the known compositions, such as Barberton or Bounce Rock, by some relatively simple igneous differentiation process but insufficient data exist to evaluate this possibility in any rigorous manner.

Another consideration is the potential role of meteoritic debris in the provenance of these sedimentary rocks. For sedimentary rocks older than about 3.8 Ga, the potential for a significant meteoritic component increases significantly. For example, on the Moon the meteoritic component of lunar soils is about 2% on average and approximates to a chondritic composition [39] and there is reason to expect that the meteoritic flux is greater for Mars at any given time [40]. On the other hand, geochemical evidence for significant meteoritic components in terrestrial sedimentary rocks older than 3.0 Ga is limited (e.g., [41]). The effect of removing from the outcrops a composition equivalent to an average CI chondritic meteorite is shown on Fig. 3. Cr/Ni ratios increase to values typical of basaltic shergottites with removal of about 6% chondritic component. However, because Meridiani igneous rocks Bounce Rock and Barberton have Cr/Ni ratios within a factor of 2 of Meridiani outcrop and Cr/Ni ratios of about 2 are not unusual for basaltic rocks in general [42], there is no requirement of a meteoritic component in the provenance.

4.3. Provenance of chemical components

Because these rocks are interpreted as reworked evaporitic sandstones with a strong diagenetic overprint, evaporitic minerals that have been identified or inferred probably do not reflect an equilibrium assemblage with respect to any single fluid and may not include all minerals that existed within this depositional system. Nevertheless, several lines of evidence indicate that chemical constituents of these rocks precipitated from fluids that were derived from the alteration of olivine-bearing or -normative basalts under low pH conditions. Evidence can be summarized as follows:

1. Identification of jarosite is strong evidence that fluids were at pH<5 since that marks the effective upper stability level of this mineral;
2. Occurrence of hematite as a diagenetic mineral suggests low pH environments. Near surface environments of Mars are thought to be oxidizing and so Fe transport would be enhanced at low pH;
3. Experimental studies of alteration of synthetic martian basalt [16,43] indicate that Mg release is greatly enhanced during dissolution of olivine-bearing basalts or olivine-normative basaltic glasses but inhibited during alteration of olivine-free (pyroxene and feldspar-dominated) basalts;
4. Fluid-rock modeling [17] suggests that the inferred evaporite and diagenetic mineral assemblages of Mg-sulfate>Fe-sulfate=Ca-sulfate and hematite can be derived from low pH fluids that have interacted with such rocks. In fluids derived from olivine-free basalts, Ca-sulfates dominate over Mg-sulfates, which does not appear to be the case at Meridiani where Mg-sulfates appear to dominate.

5. Diagenetic features

Evaporites are highly susceptible to extended and complex histories of post-depositional diagenetic processes [44,45] and the sedimentary rocks at Meridiani Planum are no exception. However, it is worth noting that, in spite of the highly reactive character of the chemical constituents, in only a few places so far observed do diagenetic processes appear to be so per-

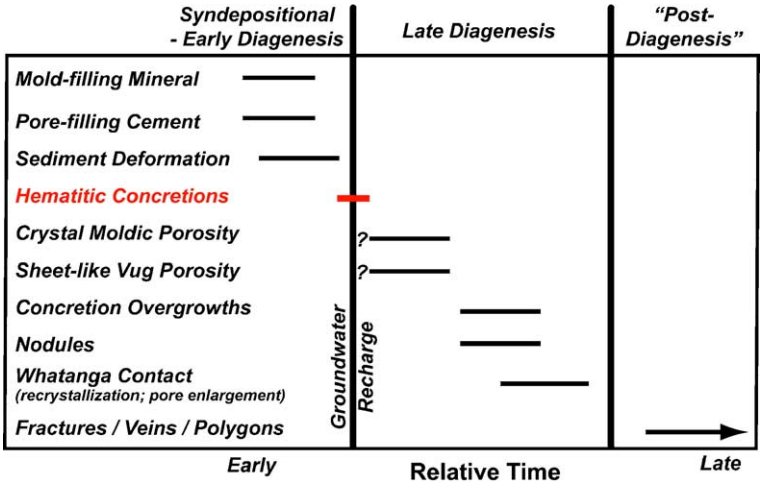

Fig. 4. Schematic diagram showing the relative timing of diagenetic features observed in the Burns formation. The boundary between early and late digenesis is arbitrarily set at the formation of the concretions because this was likely a relatively rapid event associated with a chemically distinct groundwater recharge event. See text for further discussion.

vasive as to obscure or significantly disrupt primary sedimentary fabrics (i.e., bedding, lamination, cross bedding, ripple forms). *Opportunity* imaged a variety of textures, including cements, concretions, nodules and secondary porosity that formed after deposition, and are clearly diagenetic. The inferred order of these features is summarized in Fig. 4 and Table 2.

5.1. Cements

At least two and possibly four generations of cement are present within these rocks (Fig. 5). The mineralogy of cements is not constrained but inferred to be one or more of the possible evaporitic mineral jarosites, Mg-sulfate, Ca-sulfate, other Fe-sulfates, chlorides ± hema-

Table 2
Proposed geologic history of the Burns formation (oldest to youngest)

Depositional Stage	Event
PRE-DEPOSITIONAL *(Playa Lake Facies)*	1. Deposition and evaporative cementation of basaltic mud, likely near margin of playa lake. Erosion to produce sand-sized grains.
DEPOSITIONAL *(Dune-Sand Sheet-Interdune Facies)*	2. Aeolian transport of impure evaporitic sand grains within dune - sand sheet - interdune depositional environment under a range of dry to wet conditions. Periodic rise of groundwater table results in shallow subaqueous conditions in interdune setting [2].
DIAGENETIC *(Related to syndepositional evaporation and fluctuating groundwater table)*	3. Syndepositional formation of small (mm-scale) cross-cutting crystals of an evaporite mineral more soluble than Mg-sulfates likely during evaporation of near-surface water table or capillary fringe of water table. 4. Syndepositional to very early diagenetic formation of fine-grained (<100 μm) cement filling primary porosity, likely caused by evaporation of near-surface water table or capillary fringe of water table. 5. Rapid formation of hematitic concretions likely during a chemically distinct groundwater recharge event. A thermodynamically plausible model is that hematite (or hematite precursor) forms by the breakdown of jarosite or other iron sulfate such as melanterite. 6. Formation of secondary porosity by dissolution of small tabular crystals (crystal molds) and dissolution of earlier cements to form elongate to sheet-like vugs. Possible that the secondary porosity forms as a result of concretion growth. 7. Formation of overgrowth cements around concretions under fluid-saturated conditions. In the lower and middle units (dune, lower part of sand sheet facies), this cement is more abundant and forms at nucleation sites in addition to concretions. Contact between the middle and upper units, interpreted to be a diagenetic front, is marked by a dark colored zone where primary stratification is obscured by recrystallization and secondary porosity is especially abundant.
"POST-DIAGENETIC" *(Impact, karsting(?), erosion)*	8. Formation of fractures, fracture fillings, veins and polygonal features likely associated with impact processes. May also involve very late diagenetic processes, such as karsting. 9. Erosion of units above outcrop to produce lag of concretions on plains.

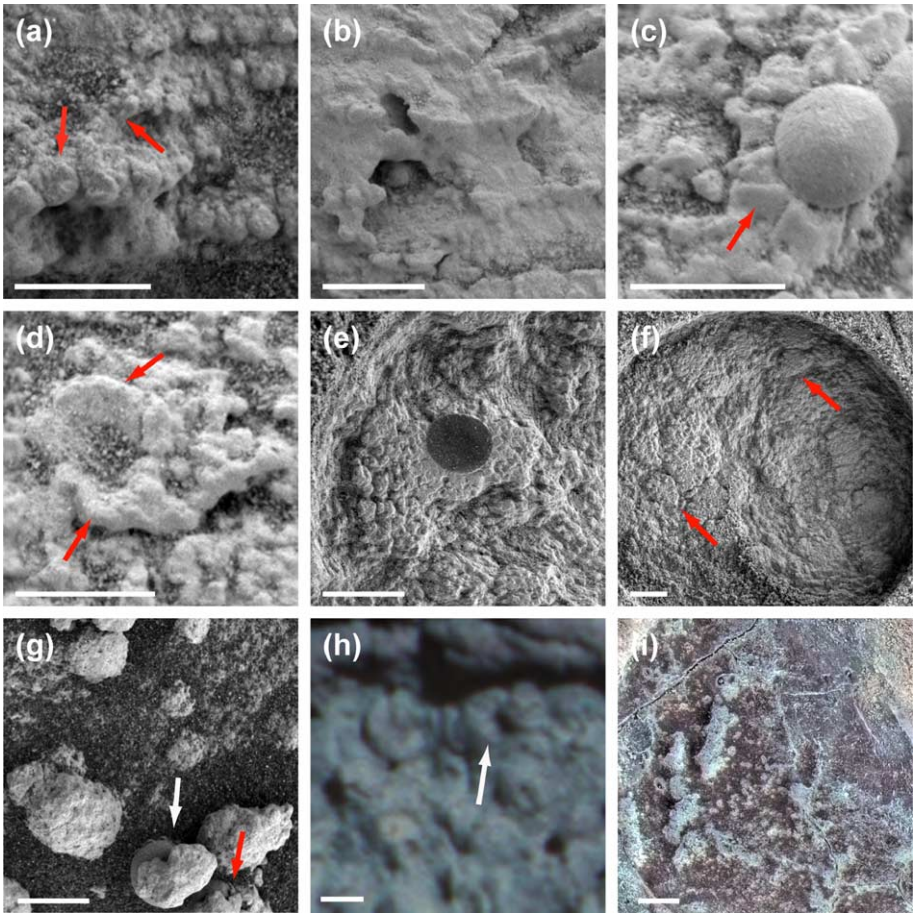

Fig. 5. MI and Pancam images illustrating the types of diagenetic cement encountered in the Burns formation (scale bars are 5 mm across). (a,b) Close up of MI images taken on Sols 42 (Flatrock) and 125 (Diogenes) showing early pore-filling cement. Note that the degree to which grain boundaries are obscured is much greater in (b) than in (a), due to a greater degree of cementation and recrystallization. (c) Close up of MI image taken in upper unit on Sol 28 (Algerita) showing isopachous blocky cements, about 2 mm thick, around spherules. (d) Close up of MI image taken in upper unit on Sol 28 (Algerita) showing zone of isopachous blocky cement where a spherule had been present but now eroded out of the outcrop. (e) MI image of abraded surface taken in middle unit on Sol 177 (Diamond Jenness, RAT-1) showing grain-cemented overgrowths on spherule. Note that in this lower part of the section, the nature of this second generation of cement differs from that in the upper unit (compare with Fig. 5c,d). (f) Part of MI mosaic of abraded rock surface (Diamond Jenness, RAT-2) taken on Sols 178 and 179. Note the nodular texture. The cementation that gives rise to this texture is assumed to be associated with the same diagenetic process that caused the overgrowths on the spherules but centered on different, indistinct nucleation sites. (g) Part of MI mosaic of soil taken on Sol 199 showing that the nodules are relatively resistant and remain intact when they erode out of the outcrop. Arrows show two of the nodules that clearly have spherules at their cores. (h) Close up of false color Pancam image of boulder Ellesmere. Note that the overgrowths on these spherules have a spoke-like appearance, suggestive of a radial fibrous texture. Concerns about rover safety precluded closer approach to confirm this possibility. This image was taken on Sol 205, sequence P2559, using 750 nm, 530 nm and 480 nm filters. (i) Part of stretched false color MI mosaic of abraded rock Lion Stone taken on Sol 108. Note that this surface is characterized by very low porosity. Based on resistance measurements collected during RAT grinding, this rock type is by far the hardest encountered in the Burns formation. See Fig. 11c,d for another example of this cement type.

tite ± amorphous silica. Cements that have been identified include the following:

1. Early fine-grained (<100 μm) pore-filling cements.
2. Cements found around spherules and in isolated nodules. In most places this cement does not obscure primary stratification, however, in the lower part of the section, and especially at the Whatanga contact separating the middle and upper units, cementation/recrystallization can be so pervasive that primary stratification is obscured.
3. Rare, *possible* isopachous radial fibrous cements around spherules. If present, they may be equivalent to blocky cements surrounding spherules (a variety of type 2), described above, but are significantly larger (see details below).

4. Possible localized cementation/recrystallization in the upper unit, leading to a reduction of porosity and hardening of the rock. This may simply be a more extensive version of the fine-grained pore-filling cements (type 1) or may represent recrystallization.

Where grains are visible on outcrop surfaces and in freshly exposed (RATed) surfaces, outlines commonly are not distinct and material with grain sizes below MI resolution (<100 μm) is present between grains (Fig. 5a). With only few exceptions, grains that can be resolved are of relatively uniform size and, consistent with cross-bedding evidence for reworking by wind and water, primary clastic grains are both well sorted and moderately well rounded. Accordingly, the fine-grained intergranular material is interpreted to be pore-filling cement rather than a separate population of fine grains. In several places there is considerable differential erosion between laminations and the cements appear to form sheets that effectively define the laminations and obscure grain boundaries. Generally, individual grains can be recognized, however, the degree to which grain boundaries are well-defined is highly variable and likely related to the amount of pore-filling cement and degree of recrystallization (Fig. 5b). The crystal sizes of these cements are below the resolution of the MI and accordingly no additional textural information is available.

A second generation of millimeter-scale cement forms around many spherules (Fig. 5c–e). In Eagle crater and the upper parts of the stratigraphic section at Endurance crater, the layer of cement typically is on the order of 1–2 mm thick and appears to be blocky and is isopachous. The formation of the overgrowths, which are significantly larger than the size of grains, resulted in a localized loss of primary fabric suggesting recrystallization of original grains and pore-filling cement. During erosion of outcrop surfaces, this cement is relatively resistant or is shielded from erosion by resistant spherules and commonly forms a pedestal to the spherules (Fig. 5c,d). The presence of isopachous cements is characteristic of the phreatic and/or capillary fringe zones in aeolian sediments that have been submerged beneath the water table [34].

Working down the stratigraphic section (top to bottom), the nature of the cement surrounding spherules changes markedly. Within the middle unit, it can reach up to 4 mm in thickness and consists of a distinctive zone of cemented sand grains that form overgrowths on the spherules (Fig. 5e,g). Where this occurs, there are also many similar-appearing nodules (Fig. 5f,g). The nodules also appear to be cemented sand grains but in this case they do not form overgrowths to spherules. Thus, although spherules form the nucleation site for a second generation of cements, lower in the section at Endurance crater, other nucleation sites must also exist because there are far more nodules than spherules.

It is possible that the isopachous blocky cements, spherule overgrowths and nodules represent multiple distinct cementation events or alternatively they could represent different expressions of fundamentally the same diagenetic process controlled by variations in porosity, permeabilty, sediment composition, grain size, fluid residence time and so forth. A complex history of cementation is characterisitc of the phreatic and capillary fringe zones in many aeolian environments because the hydrological regime can be highly dynamic in such settings [34,46].

At one location, on the rock Ellesmere near the bottom of Endurance crater there is one observation that provides *suggestive* evidence for radial fibrous textures surrounding spherules (Fig. 5h) and possibly filling fractures. The observation comes from a high-resolution Pancam image taken from several meters distance. The Microscopic Imager was unable to confirm this texture because it was not safe for the rover to approach the rock. Radial fibrous textures could form as primary cement or as a secondary recrystallization product. The second of these options is suggested because the thickness of the feature surrounding the spherule in Fig. 5h is significantly greater (about 4–5 mm) than the isopachous blocky cement described above and accordingly is likely to replace grains surrounding the spherule. In either case, such textures, if confirmed, would provide strong supporting evidence for post-depositional fluid-saturated conditions such as those found in marine or meteoric phreatic conditions [47,48].

In most places, diagenetic processes do not obscure primary sedimentary fabrics in any significant way. Two exceptions exist. At the boundary between the middle and upper units (Whatanga contact) there is a marked darkening of outcrop color (Fig. 6a,b) and depositional fabrics are obscured and in places even obliterated (Fig. 6b,c) over a zone of up to about 50 cm [2]. The pattern of diagenetic cementation and recrystallization is basically the same as elsewhere but at this location it is particularly intense and is accompanied by a large amount of secondary porosity. A similar, but somewhat less developed, zone of recrystallization also occurs about 50 cm above the Whatanga contact (see Fig. 1b). Two possible explanations are differential diagenetic effects acting on primary lithological differences, such as porosity and grain size (e.g., [49]), or a

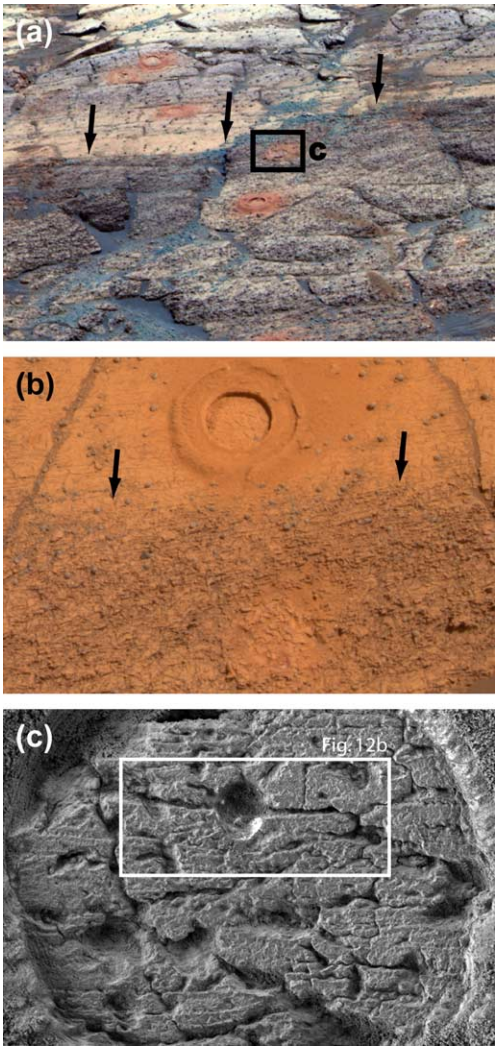

Fig. 6. (a) Close up of false color Pancam mosaic of the Burns formation in the vicinity of the Karatepe ingress path showing the distinct color change associated with the Whatanga contact (arrows), marking the boundary between the middle and upper units. Scale can be estimated from RAT holes, which are 4.5 cm in diameter. Images used in this mosaic were taken on Sol 173, sequence P2401 using 750 nm, 530 nm and 430 nm filters. (b) Close up of true color (best estimate) Pancam image of the Whatanga contact (arrows point to top of contact zone) in the vicinity of Burns Cliff. Note that laminations are highly obscured at the dark contact. Scale can be estimated from the 4.5 cm diameter RAT hole. Image was taken on Sol 310 at 12:36:29 LTST, sequence P2558, using 750 nm, 670 nm, 600 nm, 530 nm, 480 nm and 430 nm filters. (c) Close up of MI mosaic of abraded rock surface (Grindstone) taken within the Whatanga contact at the Karatepe stratigraphic section on Sol 152. Location is marked by box in (a). Note that primary stratification and grain boundaries are obscured by recrystallization and formation of secondary porosity. Also note the greatly enlarged size of the pores in the bottom half of the image. The white box shows the location of Fig. 12b.

stratigraphically controlled process that affects the intensity of diagenetic alteration. Although primary stratification is largely obscured, Grotzinger et al. [2] noted that there is no indication of facies variations in this part of the stratigraphic section and accordingly interpreted these zones of recrystallization to be the position of the top or capillary fringe of a stagnant paleo-water table, and thus diagenetic fronts.

At the top of the El Capitan outcrop in Eagle crater (Guadalupe) and in a single cobble on the Meridiani plains just outside Endurance crater (Lion Stone) RATed surfaces exposed apparently crystalline material (Fig. 5i) but with both spherules and crystal molds preserved (see Fig. 11d below). Resistance to grinding by the RAT indicates that this material is significantly harder than any other rocks encountered in the Burns formation [22]. Two possible interpretations may explain this texture. The first is that this represents a much higher degree of intergranular pore-filling cement that eliminated most of the primary porosity and thus is essentially an extreme version of cement type 1 described above. The second possibility is that this is a later pore-occluding cementing process involving recrystallization. In either case, it is worth noting that the primary sedimentary fabric (sand–silt laminations, grain boundaries) preserved on abraded surfaces at Guadalupe and Lion Stone is also much more poorly expressed than at other outcrops (see Fig. 11c below). The chemical and mineralogical composition of RATed surfaces is similar to other abraded outcrop samples [25] indicating that the processes did not introduce a significant amount of material with a composition significantly different to the main outcrops.

5.2. Spherules

Dispersed throughout the outcrop are abundant spherules (informally named “blueberries”) of relatively uniform shape and size (Fig. 7). The spherules do not appear to disrupt laminations in any significant way (Fig. 7a,b). They typically weather out of the outcrop by physical aeolian erosion and form a lag deposit on the plains surface [50] indicating that they are far more physically robust than the surrounding outcrop (Fig. 7c,d). The sizes of spherules embedded within the outcrop are rather uniform with a mean diameter of 4.2 mm (standard deviation, s.d. = 0.8 mm; 454 spherules). The spherules are almost perfectly spherical with aspect ratios averaging 1.06 (s.d. = 0.04). Volumetric densities of spherules were estimated at three locations (Shoemaker’s Patio at Eagle crater, Fram crater and in the upper unit at the Karatepe section in Endurance

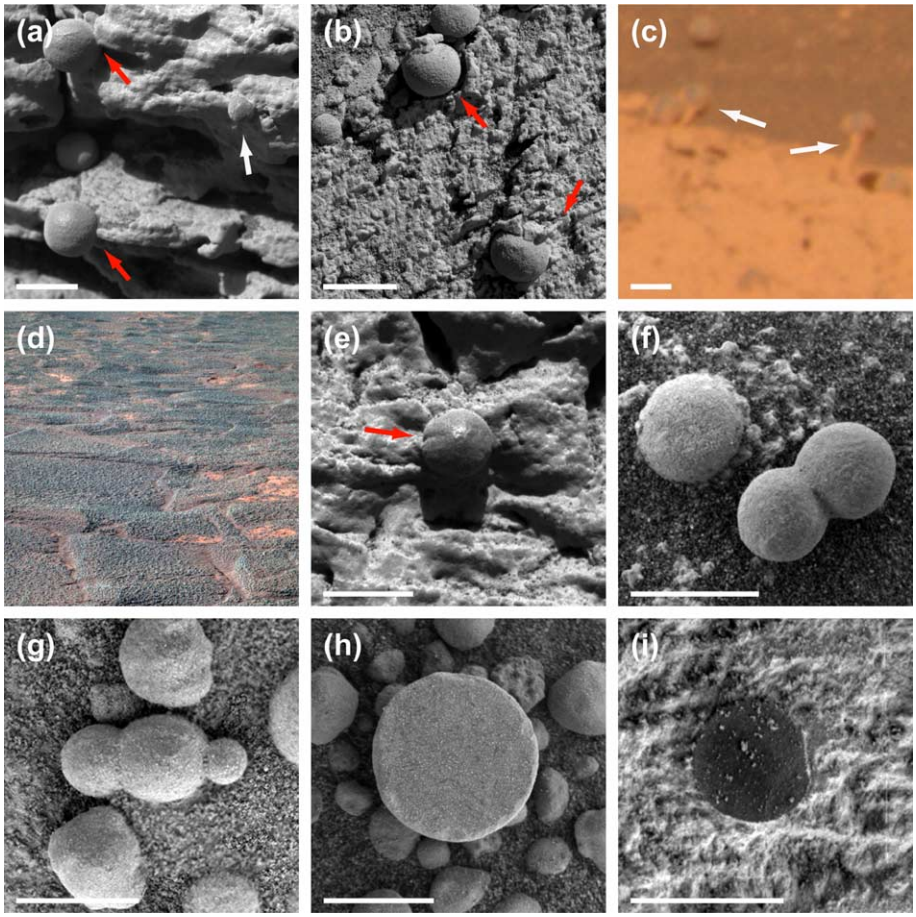

Fig. 7. MI and Pancam images of spherules in the Burns formation. Also see Figs. 5 and 11 for additional images of spherule distributions. Scale bars are 5 mm across. (a) MI image taken on Sol 39 (Last Chance) showing spherules weathering out of outcrop. Note small spherule on right hand side (white arrow) and note that laminations are not deflected by spherules (red arrows). (b) Close up of MI image taken on Sol 144 showing the lack of disruption of bedding by spherules. (c) Close up of approximate true color (best estimate) Pancam image of the rock Pilbara at Fram crater. Note that the highly resistant spherules create a "shadow" to physical erosion forming stalks. Image was taken on Sol 88 at 11:37:01 LTST, sequence P2542, using 750 nm, 670 nm, 600 nm, 530 nm, 480 nm and 430 nm filters. (d) False color Pancam image of rock-soil surface showing the concentration of weathered out spherules to form a lag deposit. Image is approximately 2 m across at the center. Image was taken on Sol 188, sequence P0050, using 750 nm, 530 nm and 430 nm filters. (e) Close up of MI image taken on Sol 28 showing the presence of latitudinal band that is contiguous with bedding. (f) Close up of MI image taken on Sol 122 showing weathered-out spherules on soil surface. Note the spherule "doublet" with conjoined spherules being of near equal size. (g) Close up of MI image taken on Sol 48 of weathered out spherules on soil surface. Note the spherule "triplet" with the central spherule being larger than the other two. (h) Close up of MI image taken on Sol 84 of spherule that has been broken in half by natural processes. Note the lack of any internal structure within the resolution capability of the MI. (i) Close up of part of MI mosaic taken on Sol 160 (Drammenfjorden) showing an abraded spherule. Note the lack of internal structure and lack of variation in albedo within the spherule.

crater, with an average of 27 spherules measured for each rock) using the formula $V=(\pi m l^2/6A)$ where m is number of spherules on a planar rock surface with area A, and l is the mean spherule diameter (i.e., the population of spherules intersected by a plane is assumed to represent what is contained within a layer of thickness l). Among these areas, volumetric density of spherules and the range of sizes differ significantly: 1.2% (s.d.=0.4%, $n=4$ rocks) at Eagle crater; 4.3 (s.d.=0.8%. $n=6$) at Fram crater and 4.0% (s.d.=2.0%, $n=6$) at Endurance crater. The overall average volumetric density is 3.2% (s.d.=2.0% for $n=17$).

A second population of spherules may exist within the soils of Meridiani Planum. This population has similar VNIR spectroscopic characteristics as the spherules within the outcrop but is of significantly smaller size, averaging 0.8 mm (s.d.=0.1 mm, $n=43$). These are not interpreted as an abraded equivalent of the outcrop spherules because they commonly maintain a

spherical shape. Instead, they may represent a different population of spherules derived from overlying outcrop material that has eroded away.

There is no evidence that spherules concentrate along any bedding feature and in a few cases they show banding or latitudinal grooves that are contiguous with surrounding bedding (Fig. 7e). The vast majority of spherules occur in isolation but rarely, they form "doublets" (Fig. 7f) and in at least two occurrences they form linear "triplets" (Fig. 7g). In some cases, the conjoined spherules are of near equal size but in other cases one of the conjoined spherules is significantly smaller than the other. Where spherule interiors are exposed, either by natural cracking (Fig. 7h) or through RAT abrasion (Fig. 7i), they show no internal structure or included grains, within the ~100 μm resolution of the MI.

The chemical composition and mineralogy of the spherules is critical to their interpretation but cannot be determined directly because they are too small to allow direct unambiguous spectroscopic measurement by any of the contact instruments. Accordingly, their composition has to be determined indirectly and thus with greater uncertainty. One indirect approach was through the "berry bowl" experiment. At an outcrop in Eagle crater there was a natural enrichment of weathered-out spherules in a small depression. Here, APXS, Mössbauer and Mini-TES measurements were made on the region of spherule enrichment and on an adjacent region apparently free of spherules. The chemical results of these experiments are shown on a ternary diagram plotting SO_3–MgO–FeO_T (Fig. 8). Also shown are analyses of soil surfaces where MI images indicated an unusual enrichment of weathered out spherules as a lag deposit or where Mössbauer indicated unusual enrichment of hematite. Because the spherule-rich region in the "berry bowl" experiment contains some amount of surrounding outcrop, extrapolation of the "unmixing" line indicates that the spherules are composed of a mixture of about 50–60% hematite (confirmed by Mössbauer and Mini-TES) and 40–50% terrigenous basaltic material that may be embedded within the spherule and/or as basaltic sand on the outcrop surface. Mixing calculations further indicate that the amount of sulfate must be below about 10% (note that jarosite was not detected by the Mössbauer spectrometer). Such simple mixing calculations likely provide a lower limit on the amount of hematite in the spherules because surface coatings on the spherules themselves are likely to result in an overestimate of the amount of basalt and sulfate. Indeed Mini-TES

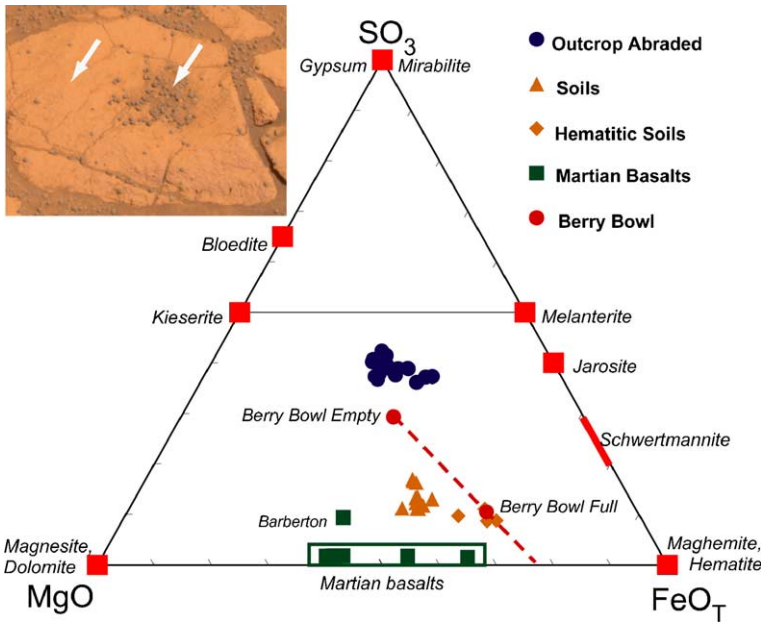

Fig. 8. Plot of mole proportions of SO_3 – MgO – FeO_T showing the results of the "berry bowl experiment" and spherule-rich soils. Note that a mixing line between spherule-rich analyses (berry bowl full) and the spherule-poor outcrop surface (berry bowl empty) extrapolates to a low sulfate composition approximately midway between average martian basalts and the FeO_T apex where hematite plots. Any surface contamination on the concretions is likely to be enriched in basaltic material and this estimate is likely a lower limit on the hematite content of the spherules. *Inset*. True color (best estimate) Pancam image of location where berry bowl experiment was carried out. Arrows point to approximate locations of "berry bowl full" and "berry bowl empty" measurements. Image was taken on Sol 45 at 10:27:51 LTST, sequence P2556, using 750 nm, 670 nm, 600 nm, 530 nm, 480 nm and 430 nm filters.

deconvolutions of spherule-rich regions suggest that they are on the order of 90% or more hematite [28], although one caveat of this analysis is that only the outer 100 μm of the spherules is being analyzed.

Hematite is distributed throughout the spherules rather than forming concentric shells or concentrating near the surface. On broken and abraded surfaces, MI images reveal no internal structure (e.g., see Fig. 7h,i). Visible through near infrared spectra show distinctive spectral responses for hematite [18] and multi-filter Pancam images of the interiors of abraded spherules indicate uniform compositions throughout.

Four possible origins were considered for the spherules: sedimentary concretions, accretionary sedimentary grains (e.g., pisolith-like), volcanic lapilli and impact glasses. The textural, mineralogical and chemical evidence is considered to be overwhelmingly consistent with these objects representing post-depositional sedimentary concretions (also see [51]). The most compelling evidence includes the following:

1. Absence of concentration along scour pits and other truncation surfaces associated with current-generated bedforms or significant stratigraphic boundaries, such as the Wellington contact, as expected for deposition of sedimentary grains, lapilli or impact glasses, where hydraulic segregation of larger and more massive grains would occur.
2. Highly distinctive composition (Fe-rich) and mineralogy (dominated by hematite) inconsistent with volcanic lapilli or impact glasses such as tektites.
3. Occurrences of “doublets” and especially linearly aligned "triplets" that are statistically unlikely in volcanic or impact environments but expected for concretions [51,52].
4. Other textural relationships, including latitudinal grooves oriented parallel to bedding, lack of significant disruption to bedding and lack of internal structure.

It is not entirely clear whether the concretions grew dominantly by replacive or displacive processes [52] although available observations would suggest that the former dominates. If the hematite content is on the order of 40–70%, with the remainder consisting of siliciclastic material, it is likely that the concretions could form by infilling of available porosity plus replacement of relatively soluble evaporitic minerals. On the other hand, if hematite makes up much more than about 70% of the concretions then it is more likely that relatively insoluble siliciclastic debris has been substantially displaced during concretion growth. Replacive processes are suggested by the complete lack of disruption of primary stratification at spherule margins.

Using 3-D terrain models generated from stereo Pancam imagery, rock boundaries and the positions of the in situ spherules (measured only from *planar* rock surfaces) were used to characterize the spatial distribution of spherules within the outcrops [53]. Nearest-neighbor (NN) distributions were calculated for the spherule positions in each rock and combined into a single distribution, shown in Fig. 9. Also shown is the mean NN distribution and standard deviation (gray region) for 500 realizations of 454 randomly-distributed positions within the 17 rock boundaries. That is, for a rock surface with p spherules, p positions were chosen at random from within the region outlined by the rock boundary. This was repeated for the remaining rocks, and the NN distribution for each case was calculated and the results combined. The entire process was repeated 500 times. The mean of the resulting distributions is plotted in Fig. 9 (dashed line). Because spherules have finite size, while choosing new spherule positions, an exclusion radius was imposed around positions already chosen in order to preclude overlap. The plotted distribution has 15 bins measuring 3.5 mm across. The last bin (with the largest value) includes all distances greater than 50 mm. A χ^2 goodness-of-fit test for 10 degrees-of-freedom (to ensure that all bins contain >5 points) yields a probability $\ll 0.001$ that the random distribution is consistent with our result. That is, a vanishingly small number of statistical realizations

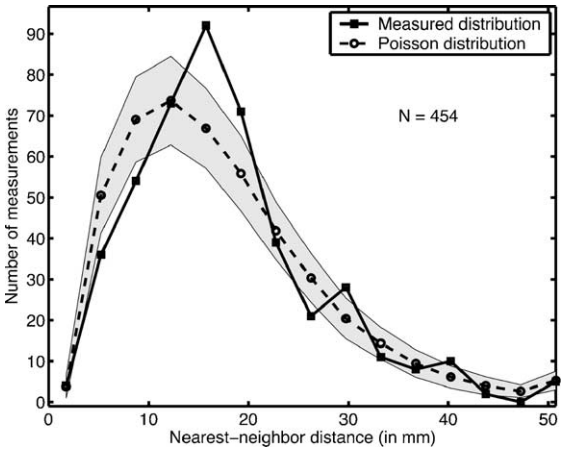

Fig. 9. Plot of Frequency versus Nearest Neighbour Distance for 454 spherules (solid line) from four locations compared to a numerical random distribution (dashed line). The gray region indicates one standard deviation for 500 realizations on flat rock surfaces with identical boundaries to those from which measurements were taken. See text for discussion.

will depart from the random NN distribution as much as the measured case.

A random distribution would imply that sites favorable for the nucleation and growth of concretions are ubiquitous and densely distributed through the rock (i.e., all sites have an equal probability of nucleating), or else that favorable sites are themselves randomly distributed. A random distribution of spherules would imply moreover that the nucleation and growth of a concretion does not change the likelihood that other concretions will nucleate nearby. Our results indicate a clear departure from a random distribution. The measured distribution lies below the random distribution for small separations, and this may imply that concretions diminish the likelihood of nucleation in their proximity (e.g., competing zones of depleted solute). Because we find examples of doubly- and triply-fused concretions (Fig. 7f,g) this interference clearly does not occur in all circumstances. An alternate explanation is that favorable sites have a heterogeneous distribution such that they occur in zones with varying abundance owing, for example, to variations in permeability and porosity. Our measurements of a slight major axis elongation (~6%) suggest that fluid transport was very slow relative to the time it took the concretions to grow. Note that this very slight major axis elongation would also include any compaction effects, although these are considered to be minimal.

The regional distribution of concretions place important constraints on their timing. Sedimentary structures indicate that both subaqueous (upper part of upper Burns unit) and aeolian (lower and middle Burns units) facies exist in this sedimentary succession [2]. Within Endurance crater, notably at Burns Cliff, compelling examples of high angle meter-scale cross beds overlain by low angle sandstones are interpreted as dune and sand sheet facies, respectively. Accordingly, an important observation is that concretions also are found in these sedimentary rocks and their distribution is unaffected by major facies boundaries (see Fig. 10). Accordingly, formation of concretions is interpreted to have been sometime after deposition of the entire sequence because the concretions are pervasively distributed across facies boundaries.

The formation of hematitic concretions is not an unreasonable process to expect in a complex and reactive iron and magnesium-rich, acidic evaporite system. The resulting evaporitic mineralogy is highly labile and stability of many of the minerals is very sensitive to pH, oxidation state, ionic strength and composition of groundwater [17,25]. Tosca et al. [17] modeled the effects of fresh water recharge on evaporites precipitated from fluids derived by interaction with olivine-bearing basalts and found that breakdown of jarosite to form goethite or hematite resulted, e.g.:

$$(H_3O)Fe_3(SO_4)_2(OH)_6 \Rightarrow 3FeO{\bullet}OH + 2SO_4^{2-} + H_2O + 4H^+. \quad (1)$$

Another plausible reaction is oxidation of a highly soluble ferrous sulfate, such as melanterite [54], a possible late-stage evaporite mineral [17] and candidate crystal mold-filling mineral (see below), to form goethite or hematite e.g.:

$$FeSO_4{\bullet}7H_2O + 0.25O_2 \Rightarrow FeO{\bullet}OH + SO_4^{2-} + 5.5H_2O + 2H^+. \quad (2)$$

Note that both of these reactions would lower the pH of the groundwater and likely move the system back in the

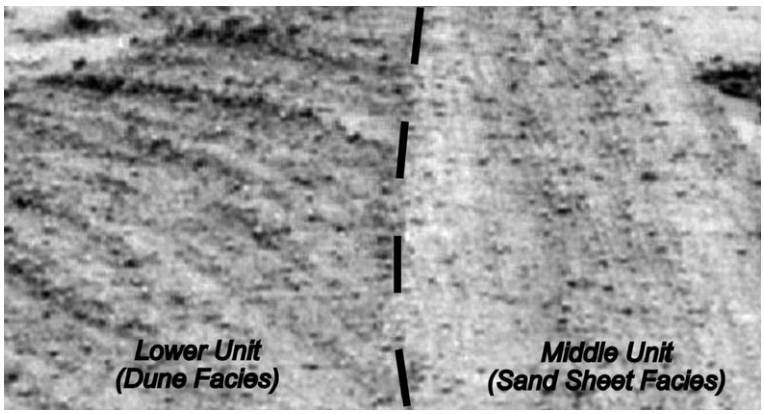

Fig. 10. Close up of grayscale "super-resolution" Pancam image showing the Wellington contact that separates the lower dune facies from the middle sand sheet facies [2]. Note the distribution of spherules on either side of the contact. The scale of the image can be estimated from the size of spherules, which average about 4.2 mm in diameter. Images used to construct this "super-resolution" picture were taken on Sol 288 using the 430 nm filter.

direction of jarosite and melanterite stability [17], thus creating a potential mechanism for abruptly shutting down the concretion-forming process. Formation of concretions by such reactions is very likely to be a major porosity-forming process. The molar volumes of jarosite and melanterite are approximately seven times that of goethite and five times that of hematite. Accordingly, depending on the exact reaction and assuming sulfate ion remains in solution, between approximately 2 and 10 cm^3 of porosity is produced for every cm^3 of goethite/hematite that is formed.

The time it takes for concretions to grow has been studied in some detail [55–58]. For the example where hematite (or a hematite precursor such as goethite) forms by breakdown of jarosite with no additional introduced material [17] the concretions would likely grow by transport-controlled replacement/precipitation [56,58]. The rate of growth would depend on concretion size, molar volume of dissolving and precipitating minerals, concentration gradients of solute in precipitating fluid around growing concretions, volume fraction of the sediment in which the concretion forms and molecular diffusion coefficients. For 4 mm concretions of goethite or hematite, that form at the expense of jarosite in a sediment with 20% porosity, ~3 ppm Fe concentration gradients (consistent with modeling of Tosca et al. [17]) and molecular diffusion rates of 10^{-5} cm/s, timescales of significantly less than 10^3 martian years are calculated, indicating very rapid formation.

In summary, diagenetic hematitic concretions embedded within the outcrops appear to have formed very rapidly under near isotropic fluid flow conditions (stagnant to very slow fluid movement). Formation of hematite by breakdown of jarosite during basin recharge by relatively dilute groundwater [17] or oxidation of ferrous sulfates, such as melanterite, are plausible mechanisms for their formation. There is no need to call on the introduction of any exotic fluid composition or any mineral that is not inferred for this geochemical system [17,25].

5.3. Secondary Porosity

Throughout much of the outcrops, void spaces of various sizes and shapes were observed. These voids typically are significantly larger than the size of framework sand grains and accordingly are interpreted to represent secondary porosity related to dissolution processes. The pores can be divided into two basic types:

1. Crystal-shaped molds. These features are equivalent to the "vugs" described in Squyres et al. [1]. For this work, the porosity nomenclature of Choquette and Pray [59] is applied and the term "vug" is restricted to non-fabric selective features.
2. Elongate to sheet-like vugs. The length to width ratios of these pores are variable but in places are greater than 10, which would indicate that this pore type grades into "channel pores" [59].

Scattered throughout the outcrops are domains containing millimeter scale crystal-shaped pores (Fig. 11). The pores typically are on the order of 0.5–1.5 mm wide and 2–8 mm long and, where present, constitute as much as 5% of the outcrop by area (Fig. 11a). Length/width ratios vary by about a factor of 3–4 (Fig. 11a,b). In many places they are lozenge or tabular shaped with sharp well-defined straight edges. In others, the edges appear corroded and the pore enlarged. In places the pores appear to preferentially align at high angles to bedding but in other places there is no clear preferred orientation. Accordingly, the pores are interpreted to represent molds of an earlier formed mineral (see below). Although no independent constraints are available on the mineral, the shapes of the pores suggest a monoclinic crystal habit. There is no evidence that the original crystal mold-filling mineral, which is significantly larger and less spherical and rounded than typical grains, significantly disrupts primary laminations.

In many places, these pores are filled with fine-grained dark material, likely fine basaltic sand. There is no textural evidence to suggest that this sandy material is derived from the outcrop itself and so it is likely that this fine-grained debris results from relatively recent accumulation by aeolian processes.

On Earth, the timing of randomly oriented euhedral evaporitic mineral growth (i.e., syndepositional vs. post-depositional) is generally considered to be ambiguous. However, for the sedimentary environments that have been proposed for these rocks (dune–sand sheet–interdune), very early diagenetic, syndepositional formation of evaporitic minerals is a common phenomenon [32,44,60–62]. Accordingly, we interpret the original crystal mold-filling mineral to be an early diagenetic mineral that formed within the sediment shortly after deposition by evaporation of pore-filling brines derived from the underlying water table or capillary fringe.

We further interpret the pores themselves to represent secondary moldic porosity [59] rather than a surficial feature caused by relatively recent wind or chemical abrasion. In places, the size of pores increases rather than decreases with depth on surfaces that have

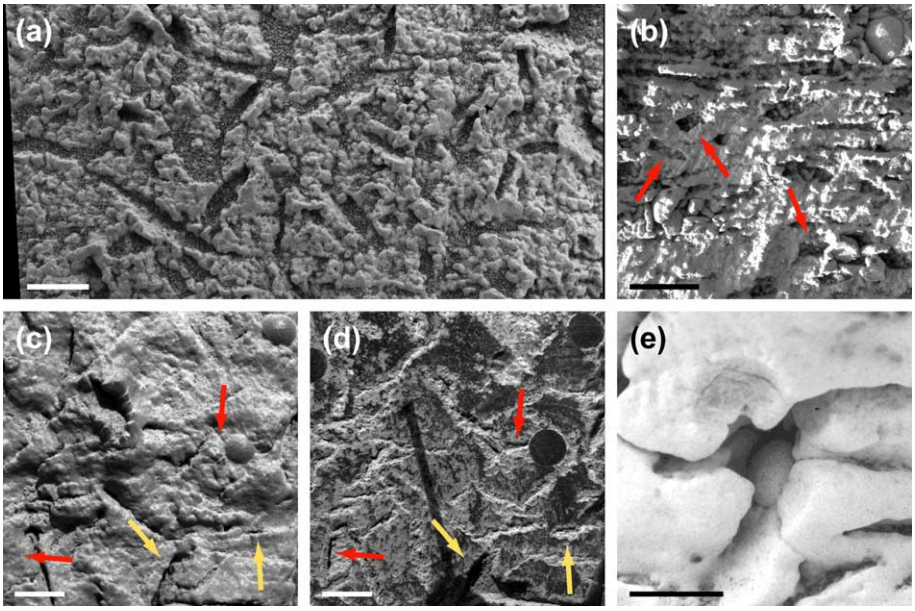

Fig. 11. MI images of crystal-shaped molds. Scale bars are 5 mm. (a) Close up of MI mosaic taken on Sol 27 (El Capitan) showing distribution of molds in the upper interdune facies. Note that the pores are elongate, commonly with sharply defined margins and angular teminations, are randomly oriented and are significantly larger than sand-sized grains. The pores are interpreted to represent secondary crystal moldic porosity. The site of the molds is interpreted to have been the original location of a highly soluble, near-euhedral evaporitic mineral that formed within the sediment during or shortly after deposition. (b) Close up of MI mosaic taken on Sol 151 (Kettlestone) showing distribution of crystal molds. Note that these molds have similar shapes as seen in (a) but that many are smaller and have lower length/width ratios (red arrows). (c), (d) Close up of MI images taken of the rock Guadalupe on Sols 34 (c) and 35 (d) showing the same field of view of pre-RAT and post-RAT surfaces. Note that in some cases molds that are present on the unabraded surface become enlarged on the abraded surface (yellow arrows) and in other cases, molds that are not observed on the unabraded surface appear on the abraded surface (red arrows). These observations are considered evidence that the molds represent intrinsic porosity in the rocks rather than a surface erosion feature. (e) Close up and highly stretched MI image taken on Sol 29 (El Capitan) showing a spherule impinging into a crystal mold. If the moldic porosity had been present when the spherule formed, it is likely that the shape of the growing spherule would have been influenced by the increased permeability. Accordingly, this cross cutting relationship is taken as evidence that the secondary porosity represented by the molds post-dates the formation of the spherules.

been abraded by the RAT (compare Fig. 11c and d). Physical abrasion is most likely to diminish its effect with depth rather than increase its effect. At the extreme, some crystal molds that are exposed after abrasion are not present on the unabraded outcrop surface (compare Fig. 11c and d). Finally, no partial or complete intact crystals of similar habit were encountered on any pristine surface or on any abraded surface.

Magnesium sulfate is one likely major evaporitic component of the outcrops and such minerals are highly soluble [25]. During diagenesis, the mold-forming crystal material consistently and fully dissolved but the surrounding evaporitic minerals appear to have remained largely intact, thus constraining the candidate crystal compositions to be a late-forming evaporitic mineral. Melanterite, a low density, hydrated ferrous sulfate is one possibility to account for the features observed. Its monoclinic crystal habits include stubby prismatic or blocky to tabular crystals. Melanterite has also been observed in acidic terrestrial environments [30,54]. Other possibilities include magnesium or iron chlorides and, less likely, glauberite, a Na–Ca sulfate.

The relative timing of the crystal molds and hematitic concretions is only partly constrained. In places crystal molds abruptly terminate against the edge of spherules (Fig. 11d) suggesting but certainly not confirming a cross cutting relationship consistent with the interpretation that the mold-forming mineral was early. The formation of the secondary moldic porosity appears to post-date formation of the hematitic concretions: in Fig. 11e, a spherule is shown impinging an empty pore, but neither filling the space nor having its spherical shape perturbed. Had no crystal been present at this point in the diagenetic history, the spherule's symmetry should have altered as it preferentially grew into the vacant space.

On many abraded surfaces large elongate to sheet-like irregular void spaces occur. These features appear to have a preferential but by no means exclusive alignment with primary bedding fabrics (Fig. 12). The scale of these features is typically millimeters to centimeters

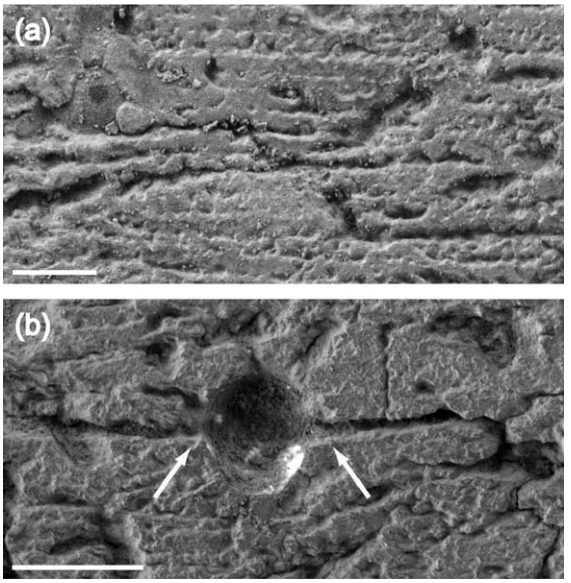

Fig. 12. MI images of elongate to sheet-like vugs. Scale bars are 5 mm. (a) Close up of part of MI mosaic of RAT abraded outcrop surface taken on Sol 145 (Cobble Hill). These features are interpreted as secondary vug porosity that resulted from dissolution of relatively soluble evaporitic components in the sedimentary rock. (b) Close up of part of MI mosaic of RAT abraded outcrop surface taken on Sol 152 (Grindstone). The surrounding region of this image, showing further examples of this type of porosity, is shown in Fig. 6c. The circular feature in the center of the image is the location of a spherule that has fallen out during the RATing operation. Note the relationship between the secondary porosity and the spherule (arrows). Although the original shape of the spherule is not known, there is no suggestion from its mold that the shape was influenced by the presence of the sheet-like vug porosity. Accordingly, it is likely that the porosity post-dates the formation of the spherules and formed at about the same time as the moldic porosity.

long and sub-millimeter to millimeters wide. They are interpreted to represent secondary vug porosity [59], likely due to the dissolution of relatively soluble evaporitic minerals. In places, the length to width ratio of these pores is greater than 10 and accordingly this vug porosity grades into channel porosity [59]. At one location a single layer of sheet-like vug porosity is observed on either side of a spherule (Fig. 12b), however, the spherule fell out during the RATing operation and the detailed cross-cutting relationship cannot be observed. The outline of the spherule socket appears to be uniform across the boundary with the sheet-like vug, suggesting that there was no secondary vug porosity at the time of spherule growth. No textural relationships have been noted to suggest any cross-cutting relationships between the secondary porosity represented by the crystal molds and sheet-like vugs and accordingly, these are interpreted to have occurred at essentially the same time and to post-date the formation of the spherules.

At the stratigraphically-controlled zones of recrystallization, typified by the Whatanga contact (Fig. 1b), the size of many of the elongate to sheet-like vugs appears to be greatly enlarged (Fig. 6), suggesting that further dissolution of pre-existing porosity and likely the formation of completely new secondary vug porosity played an important role in the development of these zones.

5.4. Disrupted bedforms

Near surface mineral growth, hydration/dehydration reactions and mineral transformations are very common during early diagenesis of evaporitic sedimentary rocks on Earth leading to post-depositional volume changes. Accordingly, evidence for synsedimentary deformation and disruption of primary depositional fabrics is common [44]. In aeolian settings, the influence of such processes is greater where chemical sedimentation dominates over clastic sedimentation and where damp to wet conditions perisist [63,64]. The preserved rocks at Meridiani Planum are thus notable for the general overall coherence of primary sedimentary fabrics such as laminations, cross beds and possible ripples, consistent with a clastic-dominated aeolian system. Only in zones of later diagenetic recrystallization, such as at the Whatanga contact and Guadalupe, are primary fabrics highly obscured.

Grotzinger et al. [2] described a facies containing wavy– to irregular-bedded sandstones within the middle and upper units of the Burns formation (see Fig. 13 in [2]). In the middle unit, these features are mainly related to clastic depositional processes however, as one moves up through the section, and especially in the upper unit, convolute to contorted bedding, massive bedding and possible teepee structures or salt-ridge structures are present within aeolian sandstones. Grotzinger et al. [2] interpreted these features to represent a combination of soft-sediment and brittle synsedimentary deformation (depending on degree of cementation) caused by mineralization and deformation associated with evaporation of brines from a near-surface water table within the interdune environment.

5.5. Other features

A variety of other features have been noted in the outcrops of Meridiani Planum that could have a diagenetic origin or influence. These include the following:

1. Meter-scale fracture patterns near the top of the Meridiani Planum outcrops (Fig. 13a,b). In many

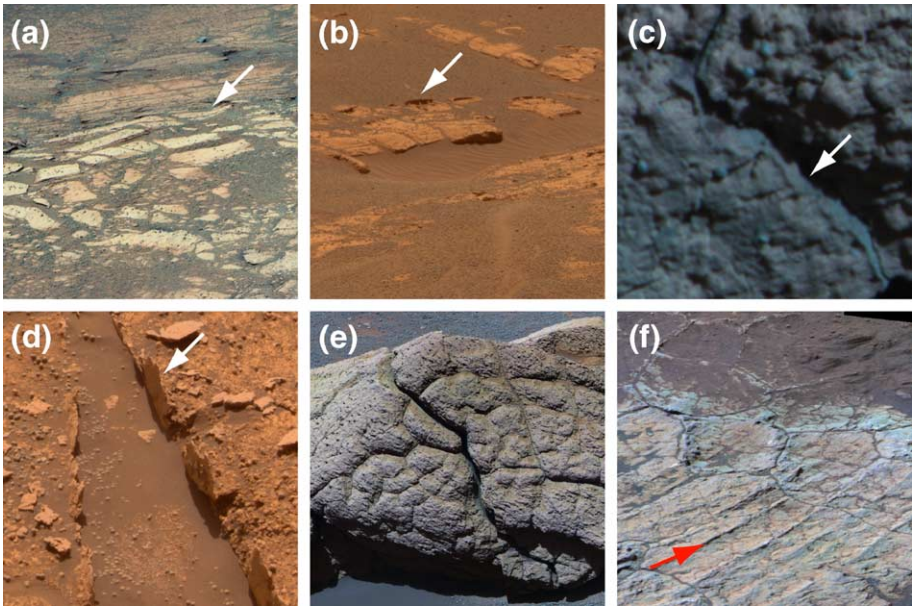

Fig. 13. Pancam images of various features that are considered to be of questionable diagenetic origin. (a) Close up of false color Pancam mosaic looking down into Endurance crater along the Karatepe ingress route. Image is approximately 1.5 m across at the center. Note the highly fractured nature of the rocks in the lower part of the image (i.e., upper part of stratigraphic section) that grades down into coherent outcrop at about the position of the arrow. False color images were taken on Sol 133, sequence P2371, using 750 nm, 530 nm and 430 nm filters. (b) Close up of true color (best estimate) Pancam image of the Anatolia depression on the Meridiani plains between Eagle and Fram craters. Image is approximately 1.6 m across at its center. Note that the fractured nature of the rocks at this location well removed from any known impact site. Also not the raised feature (arrow) that is likely the selvage of a cross-cutting vein along the margin of one of the fracture blocks (compare to (d)). Image was taken on Sol 74 at 11:53:42 LTST, sequence P2591, using 750 nm, 670 nm, 600 nm, 530 nm, 480 nm and 430 nm filters. (c) Close up of false color Pancam image of boulder Ellesmere. Note the very thin (~ 1 mm) vein that cuts across the primary stratification. Scale of the image can be estimated by the spherules that average 4.2 mm in diameter. This image was taken on Sol 205, sequence P2559 using 750 nm, 530 nm and 480 nm filters. (d) Close up of true color (best estimate) Pancam image of the feature Arnold Ziffell within Endurance crater. Image is approximately 30 cm across at its center. Note the high-standing vein-like feature or selvage. These features are commonly found along the margins of fractured blocks. Image was taken on Sol 170 at 09:11:46 LTST, sequence P2598, using 750 nm, 670 nm, 600 nm, 530 nm, 480 nm and 430 nm filters. (e) Close up of false color Pancam mosaic of rock Wopmay within Endurance crater. Image is approximately 80 cm across. Note the polygonal fracture pattern on the surface of the rock. In this image, the polygonal structures appear to be a three-dimensional network rather than simply a surface feature. Image was taken on Sol 251, sequence P2432, using 750 nm, 530 nm and 430 nm filters. (f) Close up of false color Pancam mosaic of rock Escher within Endurance crater. Image is approximately 35 cm across at the center. Note the cm-scale polygonal structures on the surface of the outcrop. The linear features (arrow) are where primary stratification intersect the rock surface and it is clear that the polygonal structures cross-cut stratification and have formed on the present-day outcrop surface. Image was taken on Sol 208, sequence P2423, using 750 nm, 530 nm and 430 nm filters.

places adjacent blocks are clearly contiguous and in general the blocks do not appear to be transported far. One important exception to this is at the rim of Endurance crater. The crater margin has eroded back some distance and many breccia blocks near the rim have slumped into the crater. In places, such as at Fram crater, disrupted blocks are upturned around the crater rim and are clearly of impact origin. However, in other places, such as the Anatolia depression, fracture patterns are present but with no evidence for a nearby impact crater (Fig. 13b). At the ingress point at Endurance crater (Karatepe section), there is clearly a downward gradation from fractured blocks to coherent outcrop (Fig. 13a).

2. Cross-cutting vein-like features that express themselves as true veins (Fig. 13c) or what appear to be differentially eroded selvages of fracture-filling veins (Fig. 13d). Many of the vein-like features that have been observed within some rocks are also found at the margins of disrupted blocks associated with meter-scale fractures.
3. Small scale polygonal textures exist on some rock surfaces in isolated out-of-place boulders within Endurance crater and on blocks preserved on the Meridiani Plains. In some places, they appear to be three-dimensional networks (Fig. 13e) but in other places, they appear to be restricted to rock surfaces (Fig. 13f). Wherever relationships can be observed, the symmetry axis of each polygon is normal to the

present-day erosional surface and thus cut across primary bedding. Accordingly, the polygonal structures post-date sedimentation and so do not represent desiccation features contemporaneous with deposition. Possible origins include impact-related fracturing, various septarian processes, synaeresis cracks, diagenetic volume changes associated with mineral transformations or dehydration, relatively recent desiccation of surface deposits that post-date the formation of the crater.

In terrestrial settings, all such features would most likely be interpreted as diagenetic in origin (e.g., [65–67]). However, on Meridiani Planum, the relationship between meteorite impact craters and outcrop exposure provides alternative explanations. Evaporitic sedimentary materials on Earth are highly prone to dissolution and karsting and incipient karsting can be difficult to distinguish from impact-related brecciation [67]. Another possibility is that the fracture patterns result from regional cracking during mineral dehydration and/or water expulsion. For example, the dehydration of hydrated magnesium and ferrous sulfate minerals, with the general formulas $MgSO_4 \bullet nH_2O$ and $FeSO_4 \bullet nH_2O$, are controlled largely by relative humidity and they lose approximately 10–15% of their volume for every water molecule removed. In any case, many of these processes are not mutually exclusive. Karsting commonly initiates along joint or fracture systems, such as those that could form on a more regional scale during impacts.

An important avenue of future research will be to map the orientation of fractures and polygonal features and compare them to regional structural features (craters, regional depressions such as Anatolia and bedding). For example, if they form a regional pattern unrelated to impact craters, it might suggest a diagenetic origin or influence.

6. Geological/diagenetic history

The provenance and diagenetic histories that can be inferred from the preserved mineralogical, chemical and textural relationships in the Burns formation are generally consistent with those expected for the dune–sand sheet–interdune depositional setting suggested by Grotzinger et al. [2]. Observed diagenetic textures dominantly reflect phreatic and capillary fringe zone environments. In this depositional setting, vadose zone diagenetic processes are most effectively preserved in the dune facies above the water table [34]. In addition, diagnostic vadose zone textures, such as meniscus and pendant cement, are commonly very fine scale and thus would be difficult to resolve by the *Opportunity* instrument suite. Such cement would also be readily overprinted by recrystallization and new mineral growth during subsequent recharge of groundwater. The contact between the lower dune and middle sand sheet facies of the Burns formation is interpreted to represent a deflation surface and thus marks erosion of the overlying vadose zone of the dunes to near the water table level [2].

The proposed geological and diagenetic history is summarized in Table 2 and Fig. 14 and discussed in greater detail below.

6.1. Syndepositional–early diagenesis

Low pH and the basaltic provenance resulted in a magnesium- and iron-rich hydrological system that produced a highly distinctive evaporitic and diagenetic mineralogy, including jarosite and hematite, Mg-sulfates and possibly other ferric and ferrous sulfates and chlorides [17,25]. There are no good terrestrial analogs that characterize both chemical and physical conditions. Iron-rich acid playa lakes are found in Australia and have some mineralogical similarities with the Burns formation, such as the presence of jarosite and hematite [15]. However, the terrigenous components of these sediments are quartzose and indeed it is the lack of buffering capacity of the associated siliciclastic sediments that permit low pH to be maintained in the Australian acid lakes. Evaporite-rich dune–interdune systems, such as those preserved in the Quaternary-aged White Sands deposits of southwestern U.S.A. [34] and the interdune sabkhas in the Saudi Arabian sand seas [32] have many physical and textural features in common with Meridiani, as does the Prungle Lake lacustrine–aeolian system of southeastern Australia [68]. On the other hand, the chemical components in these systems are dominated by Ca-sulfates and halite, typical of a high pH, iron- and magnesium-deficient evaporitic setting.

In terrestrial aeolian settings, reworking of evaporitic material that forms in penecontemporaneous, dry playa lakebeds, either as pure evaporite minerals (typically gypsum) or evaporite-cemented siliciclastic debris, commonly is the source of sand-sized grains. The large basaltic terrigenous component in the Burns formation is most readily explained by the second of these processes, thus suggesting that an active playa environment must have existed at the time of sand production [2]. Aeolian and subaqueous activity then reworked the grains into the preserved dune–sand sheet–interdune system [2].

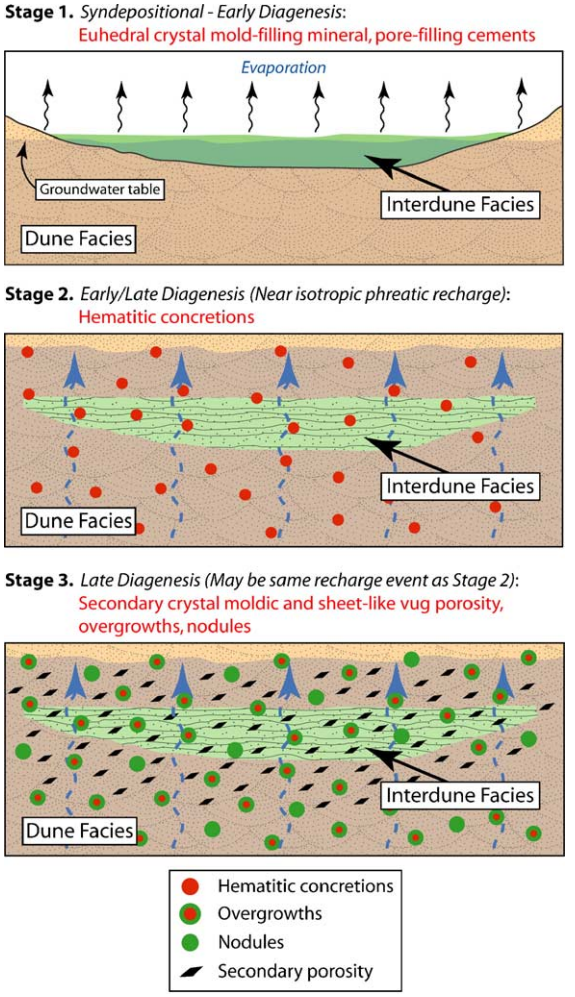

Fig. 14. Schematic model of the diagenetic history in the Burns formation. For simplicity, the sand sheet facies [2] is not represented in this diagram. *Stage 1 - Syndepositional Through Early Diagenesis*. Evaporation of near surface groundwater table or capillary fringe of groundwater table results in intrasediment formation of mm-scale euhedral crystals of highly soluble evaporite mineral. At about the same time, early pore-filling cements form by evaporative processes. *Stage 2 - Early / Late Diagenesis.* Slow recharge of chemically distinct groundwater (higher pH and/or more oxidizing than pre-existing groundwater conditions) results in breakdown of jarosite or other Fe-sulfate (such as melanterite) to form hematitic concretions. This process is likely very rapid and thus marks a convenient boundary between early and late diagenesis. *Stage 3 - Late Diagenesis*. Formation of secondary crystal moldic porosity is due to dissolution of syndepositional mm-scale euhedral evaporite crystals and secondary sheet-like vug porosity due to dissolution of relatively soluble pore-filling cements. Secondary porosity may result from formation of hematitic concretions. Second generation of cements forms as overgrowths on concretions and, lower in the section, as cemented nodules.

Pore-filling cements, likely consisting of Mg-, Fe- and Ca-sulfate ± chloride, crystallized either during or shortly after sedimentation. Cement of this nature may form by at least two mechanisms. The first is by evaporation of near surface groundwater brines (in this case Mg- and Fe-rich) resulting in crystallization of evaporitic minerals, thus implying phreatic or capillary fringe environments [34]. The second mechanism occurs in the vadose zone by dissolution/reprecipitation processes at grain boundaries or by reworking of wind-blown or adhered dust derived from eroded evaporite surface crusts and deposited with the sand [32,64]. Distinguishing phreatic from vadose zone processes requires microtextural information, such as the identification of meniscus or pendant cement textures, and cannot be resolved with available image resolution. Nevertheless, the pervasive character of these earliest pore-filling cements and evidence for complex recrystallization is considered most consistent with phreatic or capillary fringe conditions [34].

Formation of the crystal mold-filling mineral is interpreted to be analogous to the formation of relatively small euhedral halite crystals found in some modern detrital-dominated sabkhas (e.g., [34]). In this setting, halite forms distinctive layers either at the sediment surface or within the sediment itself through evaporation of the capillary fringe of a near-surface groundwater table. Meridiani mold shapes are generally similar to the crystal habit of gypsum [60], which commonly forms gypsum rosettes or "poikilitic" crystals beneath the water table [32,34,62,68,69]. Nevertheless, the crystal mold-forming mineral in the Burns formation is interpreted instead to be a very late stage evaporitic mineral (i.e., at least as soluble as Mg-sulfate), such as melanterite or an Mg-, Fe-, or Ca-chloride. The reason for this interpretation is that the dissolution of the crystal mold-forming mineral to produce secondary porosity (see below) does not appear to have caused any noticeable disruption to the immediately surrounding evaporitic components suggesting that the later dissolving fluid was nearly saturated with all but the most soluble minerals.

6.2. Late diagenesis

The formation of the hematitic concretions provides a useful benchmark separating relatively early from relatively late diagenetic processes. They likely formed very quickly, perhaps explaining their uniform size distribution, and are found pervasively across all facies boundaries. Diagenetic conditions, which are consistent with available mineralogical, geochemical and textural data [25], as well as geochemical modeling [17], are that concretions grew within the phreatic zone during slow recharge (relative to the rate of concretion growth)

of the groundwater system by a high ionic strength fluid which was more dilute than (or chemically distinct from) the original evaporite-forming fluid. Jarosite, which occurs within the sediment, is a plausible candidate for the parental evaporite mineral that could spontaneously break down to form hematite or goethite during a pH-raising recharge event [17]. An alternative possibility is that another reactive iron-rich mineral, such as the ferrous sulfate mineral melanterite, is the parental mineral and transforms to ferric oxide during recharge of more oxidizing groundwater. Although melanterite has not been identified at Meridiani, it is a plausible late stage evaporite mineral [17]. Melanterite has the advantage of being very soluble and could perhaps more readily be dissolved with little effect on the other less soluble evaporite minerals.

Throughout the sequence, concretions provide one important nucleus for the second distinct episode of cementation and accordingly this episode, which included formation of blocky isopachous cement, cemented zones around concretions and nodular textures, unambiguously post-dates formation of the concretions. Although this event post-dates the concretions, there may be no need to call on an entirely distinct groundwater recharge event. Concretions crystallized very quickly upon recharge of relatively high pH or more oxidizing groundwater. Formation of later cements and associated recrystallization, along with pore enlargement, could have occurred more gradually as the groundwater table physically subsided, at times remaining stationary to give rise to stratigraphic diagenetic fronts, such as that at the Whatanga contact.

The relative age of the secondary crystal moldic and sheet-like vug porosity is less clear-cut. Available textural evidence suggests that the secondary porosity (crystal molds and vugs) post-date the concretions. There is no textural relationship between the second generation of cements and the secondary porosity. However, in places the overgrowths on the concretions appear to post-date the sheet-like vug porosity. Where the rocks have abundant nodular textures, the secondary porosity, if originally present, is completely obliterated. Accordingly, the secondary porosity likely predates the formation of the second generation of cements. On the other hand, it is likely that these pores were greatly enlarged during formation of the diagenetic fronts represented by the Whatanga contact.

As noted above, the formation of the concretions was probably a significant porosity-forming event. The proposed reactions also lower pH and, in the case of melanterite breakdown, liberate significant amounts of water. Accordingly, an intriguing possibility is that the formation of the concretions also produces secondary porosity due to loss of jarosite or melanterite and dissolution of other relatively soluble evaporitic minerals.

Late stage features include fractures and fracture fillings, veins and polygonal fracture surfaces. Regardless of whether these features are wholly or partly diagenetic in origin or formed in response to meteorite impact processes on Meridiani Planum, these processes appear to have taken place long after deposition and burial. The presence of a lag of concretions on the Meridiani plains suggests that the modern surface is erosional and part of the stratigraphic section was removed. The presence of a second size mode of concretions in the overlying soils on Meridiani Planum also suggests that part of the eroded section was formed and/or diagenetically altered under somewhat different conditions.

6.3. Evolution of the groundwater table

Characterizing how the groundwater table within the Burns formation evolved, both physically and chemically, could have important implications for understanding the mechanisms which modulate groundwater flux during the deposition and diagenesis of the Burns formation [see discussion in [2]). The history of sedimentation and diagenesis suggests that the groundwater table evolved in a complex manner with at least four episodes of groundwater recharge taking place on the scale of the 7 m of Burns formation section studied.

The first was the infiltration of groundwater to the surface to produce the playa lake where the sand-sized grains that make up the Burns formation were formed. The top of the groundwater system must have been at high ionic strength to produce the evaporative minerals that cemented basaltic mud into sand-sized grains. The mineralogy of the evaporative cements is not known with certainty and accordingly the chemistry (notably pH, oxidation state and mineral saturation states) is not constrained. A second infiltration took place after deposition of the lower dune facies to provide the deflation surface, marking the boundary (Wellington contact) between the dune and sand sheet facies [2]. There are no chemical analyses from rocks that are unambiguously from the lower dune facies (Fig. 1b) and so it is not known with certainty if the composition of this lower unit differs from the overlying units. The best available constraints on composition of the lower Burns unit comes from MiniTES measurements that suggest the mineralogical composition of the lower Burns unit is similar to the middle and upper Burns

units (see Fig. 18 in [2]). Accordingly, there is no reason to suggest that during this recharge event, the groundwater was anything other than of generally similar composition (e.g., high ionic strength, Fe-, Mg-, Ca-rich, low pH) to later events (see below).

A third episode of groundwater recharge must have taken place to produce the cementation within the aeolian facies, culminating in the wet interdune conditions at the top of the Burns formation where subaqueous conditions prevailed [2]. It is likely that at this time the Mg-, Ca, and Fe-rich evaporative cements (including jarosite) were formed indicating that the groundwater was acidic and Mg-and Fe-rich [17,25].

A fourth recharge episode is represented by the formation of hematitic concretions. Textural evidence and geochemical modeling is consistent with the concretions forming at the expense of either jarosite or another Fe-bearing evaporative mineral (such as melanterite) during recharge of relatively high pH or more oxidizing water. Although the chemistry of the groundwater must have been different at this time, it was likely still saturated with respect to all but the most soluble evaporitic minerals since there is no textural evidence for widespread dissolution beyond the secondary porosity. Formation of diagenetic fronts represented by the Whatanga contact and other zones of recrystallization do not necessarily call for additional recharge events and these features could be related to periodic stagnation of the receding groundwater table.

In summary, the groundwater table clearly fluctuated several times, first to produce the playa lake to produce sand-sized particles and subsequently during deposition and burial of the Burns formation. For most of its history it was likely a high ionic strength, Fe-, Mg-, Ca-rich acidic brine, in order to preserve the primary sedimentary features composed of highly soluble evaporitic minerals, but on at least one occasion changed chemistry enough to produce sufficient disequilibrium to form the hematitic concretions.

7. Conclusions

The impure evaporitic sedimentary rocks preserved at Meridiani Planum preserve a remarkably complex record of depositional and post-depositional processes. The entire system of both chemical and siliciclastic components was derived from basaltic sources - terrigenous components of grains from eroded weathered basalt and chemical constituents in grains and cements from fluids generated by aqueous interaction with basalt. The grains appear to be reworked sulfate-cemented muds, thus recording a complex provenance history. The first record of this history involves an early phase of depositional mixing of basaltic and evaporative muds in a playa lake. This desiccated playa lake then served as the source of sand-sized grains which were transported by dominantly aeolian and minor subaqueous processes to form the three stratigraphic units of the Burns formation. These rocks record an extended history of syndepositional through post-depositional diagenetic alteration generally consistent with burial and periodic groundwater recharge of a dune - sandsheet - interdune depositional environment.

The Burns formation represents an extremely labile mixed siliciclastic-chemical sedimentary system. Minerals with stabilities in aqueous solutions that are extremely sensitive to modest variations in pH, ionic strength and oxidation state (e.g., jarosite, Mg-sulfates) dominate the chemical constituents of these rocks. Accordingly, it is remarkable that such a variety of complex, superimposed depositional and diagenetic textures have been so exquisitely preserved for most of the geological history of Mars.

Acknowledgements

We are truly grateful to the entire science and engineering teams on MER, numbering in the many hundreds, for making this investigation possible. We are also grateful for very helpful discussions on evaporite geology and diagenesis with Phil Choquette, Tim Lowenstein and Bill Meyers. Mary Chapman and Phil Choquette read the manuscript and journal reviews were provided by Jim Head, Noel James, Kurt Kyser and Charlotte Schreiber. All of their comments led to significant improvements and their assistance is greatly appreciated. This work was performed for the Jet Propulsion Laboratory, California Institute of Technology, sponsored by the National Aeronautics and Space Administration. The APXS and Mössbauer instruments were funded by the German space agency.

References

[1] S.W. Squyres, J.P. Grotzinger, R.E. Arvidson, J.F. Bell III, P.R. Christensen, B.C. Clark, J.A. Crisp, W.H. Farrand, K.E. Herkenhoff, J.R. Johnson, G. Klingelhöfer, A.H. Knoll, S.M. McLennan, H.Y. McSween Jr., R.V. Morris, J.W. Rice Jr., R. Rieder, L.A. Soderblom, In situ evidence for an ancient aqueous environment on Mars, Science 306 (2004) 1709–1714.

[2] J.P. Grotzinger, J.F. Bell III, W. Calvin, B.C. Clark, D. Fike, M. Golombek, R. Greeley, K.E. Herkenhoff, B. Jolliff, A.H. Knoll, M. Malin, S.M. McLennan, T. Parker, L. Soderblom, J.N. Sohl-Dickstein, S.W. Squyres, N.J. Tosca, W. Watters. Stratigraphy

and sedimentology of a dry to wet eolian depositional system, Burns formation, heridiani Planum, Mars 204 (2005) 11–72.
[3] R.E. Arvidson, F.P. Seelos IV, K.S. Deal, W.C. Koeppen, N.O. Snider, J.M. Kieniewicz, B.M. Hynek, M.T. Mellon, J.B. Garvin, Mantles and exhumed terrains in Terra Meridiani, Mars, J. Geophys. Res. 108 (E12) (2003) 8073, doi:10.1029/2002JE001982.
[4] P.R. Christensen, S.W. Ruff, Formation of hematite-bearing unit in Meridiani Planum: Evidence for deposition in standing water, J. Geophys. Res. 109 (E8) (2004), doi:10.1029/2003JE002233.
[5] B.M. Hynek, Implications for hydrologic processes on Mars from extensive bedrock outcrops throughout Terra Meridiani, Nature 431 (2004) 156–159.
[6] J.L. Bandfield, V.E. Hamilton, P.R. Christensen, A gloval view of martian volcanic compositions from MGS-TES, Science 287 (2000) 1626–1630.
[7] P.R. Christensen, J.L. Bandfield, M.D. Smith, V.E. Hamilton, R.N. Clark, Identification of a basaltic component on the martian surface from Thermal Emission Spectrometer data, J. Geophys. Res. 105 (2000) 9609–9621.
[8] H.Y. McSween Jr., T.L. Grove, M.B. Wyatt, Constraints on the composition and petrogenesis of the martian crust, J. Geophys. Res. 108 (E12) (2003) 5135, doi:10.1029/2003JE002175.
[9] P.C. van de Kamp, B.E. Leake, Petrogrography and geochemistry of feldspathic and mafic sediments of the northeastern Pacific margin, Trans. R. Soc. Edinb. Earth Sci. 76 (1985) 411–449.
[10] S.M. McLennan, S.R. Taylor, M.T. McCulloch, J.B. Maynard, Geochemcial and Nd-Sr isotopic composition of deep sea turbidites: Crustal evolution and plate tectonic association, Geochim. Cosmochim. Acta 54 (1990) 2015–2050.
[11] S.M. McLennan, S. Hemming, D.K. McDaniel, G.N. Hanson, Geochemical approaches to sedimentation, provenance, and tectonics, Spec. Pap. - Geol. Soc. Am. 284 (1993) 21–40.
[12] H.W. Nesbitt, R.E. Wilson, Recent chemical weathering of basalts, Am. J. Sci. 292 (1992) 740–777.
[13] K.M. Marsaglia, Basaltic island sand provenance, Spec. Pap. Geol. Soc. Am. 284 (1993) 41–65.
[14] D.C. Catling, A chemical model for evaporites on early Mars: possible sedimentary tracers of the early climate and implications for exploration, J. Geophys. Res. 104 (1999) 16453–16469.
[15] K.C. Benison, D.A. LaClair, Modern and ancient extremely acid saline deposits: terrestrial analogs for martian environments? Astrobiology 3 (2003) 609–618.
[16] N.J. Tosca, S.M. McLennan, D.H. Lindsley, M.A.A Schoonen, Acid-sulfate weathering of synthetic martian basalt: the acid fog model revisited, J. Geophys. Res. 109 (2003) E05003, doi:10.1029/2003JE002218.
[17] N.J. Tosca, S.M. McLennan, B.C. Clark, J.P. Grotzinger, J.A. Hurowitz, A.H. Knoll, C. Schröder, S.W. Squyres, Geochemical modeling of evaporation processes on Mars: Insight from the sedimentary record at Meridiani Planum, Earth Planet. Sci. Lett. 240 (2005) 122–148 (this issue).
[18] J.F. Bell III, S.W. Squyres, R.E. Arvidson, H.M. Arneson, D. Bass, W. Calvin, W.H. Farrand, W. Goetz, M. Golombek, R. Greeley, J. Grotzinger, E. Guinness, A.G. Hayes, M.Y.H. Hubbard, K.E. Herkenoff, M.J. Johnson, J.R. Johnson, J. Joseph, K.M. Kinch, M.T. Lemmon, R. Li, M.B. Madsen, J.N. Maki, M. Malin, E. McCartney, S. McLennan, H.Y. McSween Jr., D.W. Ming, R.V. Morris, E.Z. Noe Dobrea, T.J. Parker, J. Proton, J.W. Rice Jr., F. Seelos, J. Soderblom, L.A. Soderblom, J.N. Sohl-Dickstein, R.J. Sullivan, C. Weitz, M.J. Wolff, Pancam multispectral imaging results from the Opportunity rover at Meridiani Planum, Science 306 (2004) 1703–1709.
[19] K.E. Herkenhoff, S.W. Squyres, R.E. Arvidson, D.S. Bass, J.F. Bell III, P. Bertelsen, B.L. Ehlmann, W. Farrand, L. Gaddis, R. Greeley, J. Grotzinger, A.G. Hayes, S.F. Hviid, J.R. Johnson, B. Jolliff, K.M. Kinch, A.H. Knoll, M.B. Madsen, J.N. Maki, S.M. McLennan, H.Y. McSween Jr., J.W. Rice Jr., L. Richter, M. Sims, P.H. Smith, L.A. Soderblom, N. Spanovich, R. Sullivan, S. Thompson, T. Wdowiak, C. Weitz, P. Whelley, Evidence for ancient water on Meridiani Planum from Opportunity's microscopic imager, Science 306 (2004) 1727–1730.
[20] A.H. Knoll, M. Carr, B. Clark, D.J. Des Marais, J.D. Farmer, W.W. Fischer, J.P. Grotzinger, A. Hayes, S.M. McLennan, M. Malin, C. Schröder, S. Squyres, N.J. Tosca, T. Wdowiak, An astrobiological perspective on Meridiani Planum, Earth Planet. Sci. Lett. 240 (2005) 179–189 (this issue).
[21] B.M. Hynek, R.E. Arvidson, R.J. Phillips, Geologic setting and origin of Terra Meridiani hematite deposit on Mars, J. Geophys. Res. 107 (E10) (2002) 5088, doi:10.1029/2002JE001891.
[22] R.E. Arvidson, R.C. Anderson, P. Bartlett, J.F. Bell III, P.R. Christensen, P. Chu, K. Davis, B.L. Ehlmann, M.P. Golombek, S. Gorevan, E.A. Guinness, A.F.C. Haldemann, K.E. Herkenhoff, G. Landis, R. Li, R. Londemann, D.W. Ming, T. Myrick, T. Parker, L. Richter, F.P. Seelos IV, L.A. Soderblom, S.W. Squyres, R.J. Sullivan, J. Wilson, Localization and physical properties experiments conducted by Opportunity at Meridiani Planum, Science 306 (2004) 1730–1733.
[23] S.W. Squyres, R. Arvidson, J.F. Bell III, J. Brückner, N.A. Cabrol, W. Calvin, M.H. Carr, P.R. Christensen, B.C. Clark, L. Crumpler, D.J. Des Marais, C. d'Uston, T. Economou, J. Farmer, W. Farrand, W. Folkner, M. Golombek, S. Gorevan, J.A. Grant, R. Greeley, J. Grotzinger, L. Haskin, K.E. Herkenhoff, S. Hviid, J. Johnson, G. Klingelhöfer, A. Knoll, G. Landis, M. Lemmon, R. Li, M.B. Madsen, M.C. Malin, S.M. McLennan, H.Y. McSween, D.W. Ming, J. Moersch, R.V. Morris, T. Parker, J.W. Rice Jr., L. Richter, R. Rieder, M. Sims, M. Smith, P. Smith, L.A. Soderblom, R. Sullivan, H. Wänke, T. Wdowiak, M. Wolff, A. Yen, The Opportunity rover's Athena science investigation at Meridiani Planum, Mars, Science 306 (2004) 1698–1703.
[24] M.D. Dyar, C. McCammon, M.W. Schaefer, Roger G. Burns, Scholar and a gentleman, in: M.D. Dyar, et al., (Eds.), Mineral Spectroscopy: A Tribute to Roger G. Burns, Geochem. Soc. Spec. Publ., vol. 5, 1996, pp. xi–xiii.
[25] B.C. Clark, R.V. Morris, S.M. McLennan, R. Gellert, B. Jolliff, A.H. Knoll, S.W. Squyres, T.K. Lowenstein, D.W. Ming, N.J. Tosca, A. Yen, P.R. Christensen, S. Gorevan, J. Brückner, W. Calvin, G. Dreibus, W. Farrand, G. Klingelhoefer, H. Waenke, J. Zipfel, J.F. Bell III, J. Grotzinger, H.Y. McSween, R. Rieder, the Athena Science Team, Chemistry and mineralogy of outcrops at Meridiani Planum, Earth Planet. Sci. Lett. 240 (2005) 73–94 (this issue).
[26] R. Rieder, R. Gellert, R.C. Anderson, J. Brückner, B.C. Clark, G. Dreibus, T. Economou, G. Klingerhöfer, G.W. Lugmair, D.W. Ming, S.W. Squyres, C. d'Uston, H. Wänke, A. Yen, J. Zipfel, Chemical composition of martian rocks and soils at Meridiani Planum from the alpha particle x-ray spectrometer, Science 306 (2004) 1746–1749.
[27] G. Klingelhöfer, R.V. Morris, B. Bernhardt, C. Schröder, D.S. Rodionov, P.A. de Souza Jr., A. Yen, R. Gellert, E.N. Evlanov, B. Zubkov, J. Foh, E. Kankeleit, P. Gütlich, D.W. Ming, R. Renz, T. Wdowiak, S.W. Squyres, R.E. Arvidson, Jarosite and

hematite at Meridiani Planum form Mössbauer spectrometer on the Opportunity rover, Science 306 (2004) 1740–1745.
[28] P.R. Christensen, M.B. Wyatt, T.D. Glotch, A.D. Rogers, S. Anwar, R.E. Arvidson, J.L. Bandfield, D.L. Blaney, C. Budney, W.M. Calvin, A. Fallacaro, R.L. Fergason, N. Gorelick, T.G. Graff, V.E. Hamilton, A.G. Hayres, J.R. Johnson, A.T. Knudson, H.Y. McSween Jr., G.L. Mehall, L.K. Mehall, J.E. Moersch, R.V. Morris, M.D. Smith, S.W. Squyres, S.W. Ruff, M.J. Wolff, Mineral compositions and abundances at the Meridiani Planum site from the Mini-TES experiment on the Opportunity rover, Science 306 (2004) 1733–1739.
[29] R.V. Morris, D.W. Ming, D.C. Golden, J.F. Bell III, Occurrence of jarositic tephra on Mauna Kea, Hawaii: implications for the ferric mineralogy of the martian surface, in: M.D. Dyar , et al., (Eds.), Mineral Spectroscopy: A Tribute to Roger G. Burns, Geochem. Soc. Spec. Publ., vol. 5, 1996, pp. 327–336.
[30] D.C. Fernandez-Remolar, R.V. Morris, J.E. Gruener, R. Amils, A.H. Knoll, The Rio Tinto Basin, Spain: Mineralogy, sedimentary geobiology, and implications for interpretation of outcrop rocks at Meridiani Planum, Mars, Earth Planet. Sci. Lett. 240 (2005) 149–167 (this issue).
[31] R.L. Folk, Petrology of Sedimentary Rocks, Hemphill's, Austin, 1968, 170 pp.
[32] S.G. Fryberger, A.M. Al-Sarl, T.J. Clisham, Eolian dune, interdune, sand sheet, and siliciclastic sabkha sediments of an offshore prograding sand sea, Dhahran area, Saudi Arabia, Am. Assoc. Pet. Geol. Bull 67 (1983) 280–312.
[33] E.L. Simpson, D.B. Loope, Amalgamated interdune deposits, White Sands, New Mexico, J. Sediment. Petrol. 55 (1985) 361–365.
[34] C.J. Schenk, S.G. Fryberger, Early diagenesis of eolian dune and interdune sands at White Sands, New Mexico, Sediment. Geol. 55 (1988) 109–120.
[35] J.P. Smoot, T.K. Lowenstein, Depositional environments of non-marine evaporites, in: J.L. Melvin (Ed.), Evaporites, Petroleum, and Mineral Resources, Elsevier, Amsterdam, 1991, pp. 189–347.
[36] M.E. Sanz, J.P. Rodríguez-Aranda, J.P. Calvo, S. Ordónez, Tertiary detrital gypsum in the Madrid Basin, Spain: criteria for interpreting detrital gypsum in continental evaporitic sequences, in: R.W. Renaut, W.M. Last (Eds.), Sedimentology and Geochemistry of Modern and Ancient Saline Lakes, Soc. Econ. Pal. Mineral. Spec. Publ., vol. 50, 1994, pp. 217–228.
[37] K. Pye, Early post-depositional modification of aeolian dune sands, in: M.E. Brookfield, T.S. Ahlbrandt (Eds.), Eolian Sediments and Processes, Elsevier, Amsterdam, 1983, pp. 197–221.
[38] S.M. McLennan, Sedimentary silica on Mars, Geology 31 (2003) 315–318.
[39] E. Anders, R. Ganapathy, U. Krahenbuhl, J.W. Morgan, Meteoritic material on the Moon, Moon 8 (1973) 3–24.
[40] P.A. Bland, T.B. Smith, Meteorite accumulation on Mars, Icarus 144 (2000) 21–26.
[41] B.M. Simonson, B.P. Glass, Spherule layers - records of ancient impacts, Annu. Rev. Earth Planet. Sci. 32 (2004) 329–361.
[42] Basaltic Volcanism Study Project, Basaltic Volcanism on the Terrestrial Planets, Pergamon, New York, 1981, 1286 pp.
[43] J.A. Hurowitz, S.M. McLennan, D.H. Lindsley, M.A.A. Schoonen. Experimental epithermal alteration of synthetic Los Angeles meteorite: Implications for the origin of martian soils and the identification of hydrothermal sites on Mars, J. Geophys. Res. 110, E07002, doi:10.1029/2004JE002391.
[44] L.A. Hardie, T.K. Lowenstein, R.J. Spencer, The problem of distinguishing between primary and secondary features in evaporites, 6th Internat'l Symp. on Salt, vol. 1, 1985, pp. 11–39.
[45] B.C. Schreiber, M. El Tabakh, Deposition and early alteration of evaporites, Sedimentology 47 (Supplement 1) (2000) 215–238.
[46] G. Kocurek, N.I. Robinson, J.M. Sharp Jr., The response of the water table in coastal aeolian systems to changes in sea level, Sediment. Geol. 139 (2001) 1–13.
[47] A.C. Kendall, Radiaxial fibrous calcite: a reappraisal, in: N. Scheidermann, P.M. Harris (Eds.), Carbonate Cements, Soc. Econ. Paleontol. Mineral. Spec. Publ., vol. 36, 1985, pp. 59–77.
[48] M.E. Tucker, V.P. Wright, Carbonate Sedimentology, Blackwell, Oxford, 1990, 482 pp.
[49] R.C. Bathurst, Diagenetically enhanced bedding in argillaceous platform limestones: stratified cementation and selective compaction, Sedimentology 34 (1987) 749–778.
[50] L.A. Soderblom, R.C. Anderson, R.E. Arvidson, J.F. Bell III, N.A. Cabrol, W. Calvin, P.R. Christensen, B.C. Clark, T. Economou, B.L. Ehlmann, W.H. Farrand, D. Fike, R. Gellert, T.D. Glotch, M.P. Golombek, R. Greeley, J.P. Grotzinger, K.E. Herkenhoff, D.J. Jerolmack, J.R. Johnson, B. Jolliff, G. Klingelhöfer, A.H. Knoll, Z.A. Learner, R. Li, M.C. Malin, S.M. McLennan, H.Y. McSween, D.W. Ming, R.V. Morris, J.W. Rice Jr., L. Richter, R. Rieder, D. Rodionov, C. Schröder, F.P. Seelos IV, J.M. Soderblom, S.W. Squyres, R. Sullivan, W.A. Watters, C.M. Weitz, M.B. Wyatt, A. Yen, J. Zipfel, The soils of Eagle crater and Meridiani Planum, Science 306 (2004) 1723–1726.
[51] M.A. Chan, B. Beitler, W.T. Parry, J. Ornö, G. Komatsu, A possible terrestrial analogue for haematite concretions on Mars, Nature 429 (2004) 731–734.
[52] J. Sellés-Martínez, Concretion morphology, classification and genesis, Earth-Sci. Rev. 41 (1996) 177–210.
[53] R. Raiswell, N.J. White, Spatial aspects of concretionary growth in the upper Lias of northeast England, Sediment. Geol. 20 (1978) 291–300.
[54] F. Frau, The formation-dissolution-precipitation cycle of melanterite at the abandoned pyrite mine of Genna Luas in Sardinia, Italy: environmental implications, Miner. Mag. 64 (2000) 995–1006.
[55] R.A. Berner, Rate of concretion growth, Geochim. Cosmochim. Acta 32 (1968) 477–483.
[56] R.A. Berner, Early Diagenesis: A Theoretical Approach, Princeton Univ. Press, Princeton, 1980, 241 pp.
[57] M. Wilkinson, M.D. Dampier, The rate of growth of sandstone-hosted calcite concretions, Geochim. Cosmochim. Acta 54 (1990) 3391–3399.
[58] A.C. Lasaga, Kinetic Theory in Earth Sciences, Princeton Univ. Press, Princeton, 1998, 811 pp.
[59] P.W. Choquette, L.C. Pray, Geologic nomenclature and classification of porosity in sedimentary carbonates, Am. Assoc. Pet. Geol. Bull. 54 (1970) 207–250.
[60] R.D. Cody, A.M. Cody, Gypsum nucleation and crystal morphology in analog saline terrestrial environments, J. Sediment. Petrol. 58 (1988) 247–255.
[61] S.G. Fryberger, Role of water in eolian deposition, in: S.G. Fryberger, et al., (Eds.), Modern and Ancient Eolian Deposits: Petroleum Exploration and Production, Rocky Mountain Section, Soc. Econ. Paleontol. Mineral., Denver, 1990, pp. 5-1–5-11.
[62] M.R. Rosen, J.K. Warren, The origin and significance of groundwater-seepage gypsum from Bristol Dry Lake, California, USA, Sedimentology 37 (1990) 983–996.

[63] T.S. Ahlbrandt, S.G. Frybergerr, Sedimentary features and significance of interdune deposits, in: F.G. Ethridge, R.M. Flores (Eds.), Recent and Ancient Nonmarine Depositional Environments: Models for Exploration, Soc. Econ. Paleon. Mineral. Spec. Publ., vol. 31, 1981, pp. 293–314.

[64] L.F. Krystinik, Early diagenesis in continental eolian deposits, in: S.G. Fryberger, et al., (Eds.), Modern and Ancient Eolian Deposits: Petroleum Exploration and Production, Rocky Mountain Section, Soc. Econ. Paleontol. Mineral., Denver, 1990, pp. 8-1–8-11.

[65] G. Kocurek, R.E. Hunter, Origin of polygonal fractures in sand, uppermost Navajo and Page Sandstones, Page, Arizona, J. Sediment. Petrol. 56 (1986) 895–904.

[66] P.W. Choquette, N.P. James, Introduction, in: N.P. James, P.W. Choquette (Eds.), Paleokarst, Springer-Verlag, New York, 1988, pp. 1–21.

[67] G.M. Friedman, Dissolution-collapse breccias and paleokarst resulting from dissolution of evaporite rocks, especially sulfates, Carbon. Evapor. 12 (1997) 53–63.

[68] J.W. Magee, Late Quaternary lacustrine, groundwater, aeolian and pedogenic gypsum in the Prungle Lakes, southeastern Australia, Palaeogeogr. Palaeoclimatol. Palaeoecol. 84 (1991) 3–42.

[69] D.J.J. Kinsman, Modes of formation, sedimentary associations, and diagnostic features of shallow water and supratidal evaporites, Am. Assoc. Pet. Geol. Bull. 53 (1969) 830–840.